IEEE Access
Multidisciplinary | Rapid Review | Open Access Journal

Received August 21, 2020, accepted September 12, 2020, date of publication September 18, 2020, date of current version October 1, 2020.

Digital Object Identifier 10.1109/ACCESS.2020.3025190

Recognition of Complex Power Quality Disturbances Using S-Transform Based Ruled Decision Tree

OM PRAKASH MAHELA[1], (Senior Member, IEEE), ABDUL GAFOOR SHAIK[2], (Member, IEEE), BASEEM KHAN[3], (Member, IEEE), RAJENDRA MAHLA[4], (Student Member, IEEE), AND HASSAN HAES ALHELOU[5], (Member, IEEE)

[1]Power System Planning Division, Rajasthan Rajya Vidyut Prasaran Nigam Ltd., Jaipur 302005, India
[2]Department of Electrical Engineering, IIT Jodhpur, Jodhpur 342037, India
[3]Department of Electrical and Computer Engineering, Hawassa University, Awassa 3870005, Ethiopia
[4]Department of Electrical Engineering, National Institute of Technology at Kurukshetra, Kurukshetra 136119, India
[5]Department of Electrical Power Engineering, Faculty of Mechanical and Electrical Engineering, Tishreen University, 2230 Latakia, Syria

Corresponding author: Hassan Haes Alhelou (h.haesalhelou@gmail.com)

ABSTRACT Deteriorated quality of power leads to problems, such as equipment failure, automatic device resets, data errors, failure of circuit boards, loss of memory, power supply issues, uninterrupted power supply (UPS) systems generate alarm, corruption of software, and heating of wires in distribution network. These problems become more severe when complex (multiple) power quality (PQ) disturbances appear. Hence, this manuscript introduces an algorithm for identification of the complex nature PQ events in which it is supported by Stockwell's transform (ST) and decision tree (DT) using rules. PQ events with complex nature are generated in view of IEEE-1159 standard. Eighteen different types of complex PQ issues are considered and studied which include second, third, and fourth order disturbances. These are obtained by combining the single stage PQ events such as sag & swell in voltage, momentary interruption (MI), spike, flicker, harmonics, notch, impulsive transient (IT), and oscillatory transient (OT). The ST supported frequency contour and proposed plots such as amplitude, summing absolute values, phase and frequency-amplitude obtained by multi-resolution analysis (MRA) of signals are used to identify the complex PQ events. The statistical features such as sum factor, Skewness, amplitude factor, and Kurtosis extracted from these plots are utilized to classify the complex PQ events using rule-based DT. This is established that proposed approach effectively identifies a number of complex nature PQ events with accuracy above 98%. Performance of the proposed method is tested successfully even with noise level of 20 dB signal to noise ratio (SNR). Effectiveness of the proposed algorithm is established by comparing it with the methods reported in literature such as fuzzy c-means clustering (FCM) & adaptive particle swarm optimization (APSO), Wavelet transform (WT) & neural network (NN), spline WT & ST, ST & NN, and ST & fuzzy expert system (FES). Results of simulations are validated by comparing them with real time results computed by Real Time Digital Simulator (RTDS). Different stages for design of complex PQ monitoring device using the proposed approach are also described. It is verified that the proposed approach can effectively be employed for design of the online complex PQ monitoring devices.

INDEX TERMS Complex nature PQ event, power quality, ruled decision tree, Stockwell's transform, statistical feature.

I. INTRODUCTION

Nowadays, power quality is becoming a serious issue to service providers and consumers. This includes fluctuations in frequency, amplitude and phase of the signals of voltage and current due to wide spread application of loads with non-linear natures. These include solid-state devices, drives with adjustable speed, energy efficient lamps, power electronic controller operated devices, computers, loads used for processing of data, rectifiers and inverters used in industrial

The associate editor coordinating the review of this manuscript and approving it for publication was Eklas Hossain.

applications as well as power system faults [1]. Further, penetration of the renewable energy (RE) into the electrical system also deteriorates the quality of power [2]. Quality of electrical power is degraded due to frequently observed events such as sag associated to voltage, swell associated to voltage, MI, harmonics, flicker, spike, notch, oscillatory, and impulsive transients [3]. Simultaneous occurrence of two or more these events is considered as complex PQ event. Degraded PQ causes heating in transmission and distribution lines, malfunction of equipments and protective devices, motor failures, loss of computer data, mis-function of electronic based control systems, reduces life of equipments/appliances, reduces accuracy of meters, and causes interference with communication systems [4], [5]. In order to improve quality of power, sources of PQ events are required to be investigated so that appropriate mitigation action may be initiated. This needs that PQ events are detected, localized, classified, and monitored at fast rate and in reliable manner.

The signal processing and intelligent approaches have been utilized to recognize the PQ events [6]. Recently, analysis of PQ events in frequency domain is becoming popular. Information of time and frequency pertaining to the waveform of disturbance can effectively be extracted with the help of short-time Fourier transform (STFT) using a shifting window. Main limitation of STFT is the window with constant size which is used to identify all the frequencies available with the signal. This makes the STFT unsuitable for transient signal analysis [7]. Wavelet transform (WT) as well as its variant discrete wavelet transform (DWT) overcome drawbacks of STFT and provide representation of signals of non-stationary nature on the time-scale instead of time-frequency. However, its performance is significantly degraded when noise is associated with the signal [8]. Stockwell transform (S-transform) uses a moving Gaussian window which can be localized on scalable basis. This window combines features of WT as well as STFT. This can be converted from time domain to the frequency domain on full transformation basis. Subsequently, it can also be converted to Fourier frequency domain. S-transform uses a window for analysis of signal which is effective to decrease the width in accordance with the frequency components associated with the signal. It also provides frequency-dependent resolution of the signal. ST is capable to obtain amplitude with reasonable accuracy. This is also effective to obtain phase spectrum of the signal being analysed even when noise of significant high level is present [9].

Distinctive features obtained by filtering the PQ signal using a suitable signal processing tool are considered as input to a module of trained classifier which identifies and classifies the disturbances. Recently, large number of methods such as probabilistic neural network [10], modular neural network [11], binary feature matrix method [12], neural network (NN) [13], feed-forward neural network (FFNN) [8], Fuzzy c-means (FCM) clustering algorithm and adaptive particle swarm optimization (APSO) [1], fuzzy expert system (FES) [14], image processing [15] and extreme learning machine [16] have been proposed for classifying the PQ disturbances. A decision support tool known as decision tree (DT) functions using the graph of binary tree used to extract the hidden relation among the input and output. This is based on decisions taken following a DT starting from root to leaf nodes. Final response is associated with terminal node which is the leaf node. A DT using rules, takes the decision using a set of rules which is supported by the data with low computational burden [17].

In network of utility, more disturbances might occur at same time which is designated as complex PQ disturbance. Recently, complex PQ disturbances are observed in the utility grid due to high penetration of uncertain and variable nature renewable power generation. Most of the methods proposed in literature are applied to identify single stage PQ events. Hence, efficiency of these techniques might be limited. Therefore, in recent years researchers are focussed on recognition of complex PQ events. Hence, it is concluded that efficient devices which are effective for monitoring of the complex PQ disturbances are required. This has been considered as key factor for the proposed study and following are main contribution of the manuscript:

- Design a generalized technique using a combination of ST and DT supported by rules, using minimum features, to recognize the complex PQ issues. This is proposed to be utilized in designing the online complex PQ monitoring devices.
- A hybrid combination of ST based feature plots such as frequency contour, amplitude plot, summing absolute magnitude plot, phase plot and amplitude-frequency plot is effectively utilized to identify the PQ events of complex nature. The summing of absolute values plot proposed for identification of the complex PQ events is specific contribution of this work. This helped in achieving high efficiency of devices used for monitoring of the complex PQ events.
- Optimal set of features extracted from the ST based plots are used to design the rules for rule based DT to classify the complex nature PQ events. This has improved the PQ classification accuracy.
- This technique has merits of minimum burden of computation and good efficiency. Hence, proposed technique is suggested to design fast and accurate device for online monitoring of complex PQ events. This is also effective even when renewable power generation is available.
- Performance of algorithm is also effective even in the noisy environment with high level of noise up to 20 dB SNR (signal to noise ratio).
- Results of simulation are validated by a comparative study between the real time results computed using RTDS and simulation results. Performance of the proposed algorithm is found to be effective compared to the methods reported in literature.
- Important stages involved in design of the complex PQ monitoring device based on proposed algorithm are also formulated.

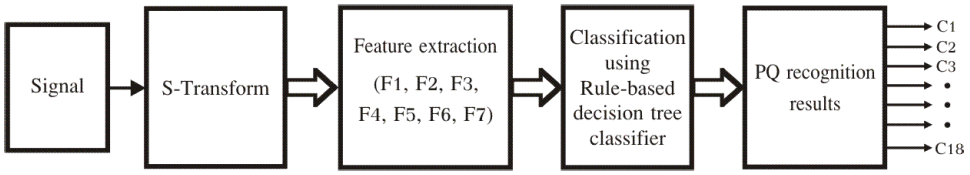

FIGURE 1. Complex PQ disturbances recognition methodology.

This article is structured in ten sections. Introduction and main contributions are described in Section I. Research work related to the recognition of PQ disturbances is discussed in Section II. Proposed approach used for recognition of the complex PQ disturbances is described in Section III. It also includes, the mathematical tools used for designing the algorithm. Section IV, presents the results for analysis of the second order, third order and fourth order complex PQ disturbances. A brief description of the S-transform supported features of complex PQ disturbances has been given in Section V. Results for classification of complex PQ events using the rule-based decision tree are presented in the Section VI. Validation of the results in real time is discussed in the Section VII. Section VIII, details the study for performance comparison of the proposed approach with the algorithms reported in literature. It also includes a comparative study of PQ classifiers. A brief discussion on procedure for implementation of the proposed method in the PQ monitoring devices has been presented in Section IX. Finally, Section X concludes the research work.

II. RELATED WORK

The researchers have proposed various techniques and algorithms for identification and classification of the PQ events. These methods reported in the literature are discussed in this section. A method using S-transform and DT using rules for identification and to classify the single stage (simple nature) PQ events is presented by authors in [18]. A technique using the ST and FCM for assessment of PQ issues associated with the utility grid network, in the presence of wind energy, is reported in [19]. In this research work, PQ events associated with the operational events such as outage and grid integration of the wind plant are investigated. In [20], authors introduced a technique to classify the single stage PQ disturbances using FCM based on features computed using ST from time-frequency representation of the disturbances. Zhong *et al.* [21], proposed a method for recognition of the PQ events using ST and DT. This study is limited for recognition of the single stage and second order complex PQ events. This method is effective for identification of the PQ events in the presence of noise level of 30-50dB SNR. This method has not been tested for higher noise level of 20dB SNR. A Stockwell transform based technique for identification of PQ events associated with the distribution network in the presence of wind energy, during different operational conditions, is available in [22]. An image enhancement approach for recognition of the PQ disturbances is reported in [23]. This approach has efficiency higher compared to the empirical mode decomposition (EMD) method. Mahela and Shaik [24], introduced a technique which is making use of the Stockwell transform and DT initialized FCM clustering for identification and to classify the single stage PQ events. A hybrid model for identification of the complex PQ events by the use of wavelet multi-class support vector machine (SVM) is detailed by the authors in [25]. Lima *et al.* [26], proposed a technique based on independent component analysis (ICA) for analysis of the complex PQ signals. Dalai *et al.* [27], introduced a cross wavelet aided Fischer linear discriminate processing technique to sense simultaneous incidence of the complex PQ events.

III. METHODOLOGY OF COMPLEX PQ DISTURBANCES RECOGNITION

The online PQ monitoring devices continuously monitor the patterns and detect the patterns which are deviated from the pure sinusoidal waveform patterns. Hence, based on the nature and shape of the patterns types of the PQ disturbances can be detected. Therefore, recognition of various patterns of the complex PQ disturbances will help to design online monitoring device for identification and to classify complex PQ events. The methodology proposed to recognize the complex PQ events is illustrated in Fig. 1. Complex PQ events are generated in accordance with the IEEE-1159 standard which realizes data in real time and used to establish generalization capacity of classifier [28]. Different combinations of numerical models of PQ disturbances reported in [29] and provided in Appendix are utilized for generating complex PQ events using programming in MATLAB 2015b software. Standard matlab codes for trigonometric and exponential functions have been utilized for generating data set of PQ events. A signal of length 10 cycles (with 50 Hz) is processed at sampling frequency of 3.2 kHz. The class symbols C1 to C18 assigned to the complex PQ disturbances and their order of complexity are illustrated in Table 1. These signals with complex PQ events are processed using multi-resolution analysis (MRA) supported by S-transform for computing a matrix known as S-matrix (complex in nature). Rows of this matrix correspond to frequency and columns to time. Every column indicates frequencies associated with signal at a moment of time. Every row indicates magnitude of frequency components with respect to time. The information associated with amplitude, frequency and phase is evaluated from ST matrix. Locus of the maximum magnitude computed from S-matrix

TABLE 1. Description of Complex PQ Disturbances.

S. No.	Name of PQ event	Class Symbol	Order of complexity
1	Sag in voltage with harmonics	C1	Two
2	Swell in voltage with harmonics	C2	Two
3	MI combined with harmonics	C3	Two
4	Flicker combined with harmonics	C4	Two
5	Voltage sag with oscillatory transient (OT)	C5	Two
6	Voltage swell with OT	C6	Two
7	Flicker with OT	C7	Two
8	Harmonics with OT	C8	Two
9	Sag in voltage with IT	C9	Two
10	Swell in voltage with IT	C10	Two
11	Flicker with IT	C11	Two
12	Harmonics with IT	C12	Two
13	Sag in voltage with spike	C13	Two
14	Sag in voltage with notch	C14	Two
15	Sag in voltage with OT and harmonics	C15	Three
16	Swell in voltage with OT and harmonics	C16	Three
17	Flicker with IT and harmonics	C17	Three
18	Sag in voltage with OT, harmonics and IT	C18	Four

at definite time is magnitude contour. For computing phase from S-matrix, the phase associated with regions of highest amplitude is evaluated. Frequency components associated with signal are also computed from ST matrix and plotted as contour of frequency [30].

Features F1 to F7 (detailed in Table 2) are computed from S-transform supported plots and used for designing rules for DT to classify complex PQ disturbances. Description of these features has been included in the Section V. These features have single valued data (refer Table 3) which are considered as input data set for programming of the decision tree supported rules to classify the disturbances. Impact of noise on performance of the classification is investigated with 20 dB SNR noise. Further, at a higher noise level of 10dB SNR the powers of signal and noise become equal. Generally, this condition is not observed in the network of distribution system because the power handled by the network is high. Hence, the noise observed in the distribution system ranges from 20dB SNR to 100dB SNR where 20dB SNR noise level is highest. Hence, 20dB SNR is selected for testing the proposed algorithm. This algorithm is effective for 20-100dB SNR range of noise level. A set of 100 signals for each PQ disturbance is prepared using the mathematical formulation detailed in Appendix. This data set is computed by the variation of different parameters of every PQ disturbance such as frequency, amplitude, phase etc. The 70 data of each PQ disturbance are used for training the DT and 30 data of each PQ disturbance are used for testing the DT classification approach. Performance of the proposed DT based classifier is compared with the base line classifiers including OneR, ZeroR and Decision stump.

TABLE 2. Description of Features Used for DT Rules.

S. No.	Symbol of Feature	Description of Feature
1	F1	Sum factor
2	F2	Skewness of phase curve
3	F3	Amplitude factor
4	F4	Kurtosis of the amplitude curve
5	F5	Kurtosis of the phase plot
6	F6	Kurtosis computed from summing of absolute values plot
7	F7	Kurtosis computed from amplitude-frequency plot

Results of simulation are validated by comparison with results in real time computed using the RTDS. Mathematical relations of the Stockwell transform utilized for recognition of complex PQ events and used for design of the PQ monitoring devices are provided in the following subsection.

A. STOCKWELL TRANSFORM

ST is a hybrid combination of the STFT and WT which contains features of both and considered in a separate group. This had been introduced in the year 1996 by the R. G. Stockwell. ST computes MRA of a signal in time domain and retains absolute phase of every frequency component. This has used a window, the width of which changes in inverse ratio of frequency. This effectively provides high resolution of time for high frequencies and high resolution for lower frequencies [31]. Most of the complex PQ events are non-stationary and ST effectively extracts features using scalable and localized Gaussian Window which is dilating and translating [32]. The continuous WT (CWT) of the function $h(t)$ is computed using below detailed relation [32].

$$W(\tau, d) = \int_{-\infty}^{\infty} h(t) w(t - \tau, d) dt \tag{1}$$

where $W(\tau, d)$: mother wavelet (it may be replica on a suitable scale), d: dilation which represents width of wavelet used for controlling resolution. Dilation factor is considered as reciprocal of frequency. Translation parameter (τ) is used to control position of the Gaussian window (GW) on time axis.

ST used to process a signal $h(t)$ is basically a CWT using a suitable mother wavelet which is multiplied by a factor of phase.

$$S(\tau, d) = W(\tau, d) e^{-i2\pi f \tau} \tag{2}$$

Here, mother wavelet can be computed using the following relation.

$$w(t, f) = \frac{|f|}{\sqrt{2\pi}} e^{-\frac{t^2 f^2}{2}} \tag{3}$$

Continuous ST can be computed using the following relation.

$$S(\tau, f) = \int_{-\infty}^{\infty} h(t) \frac{|f|}{\sqrt{2\pi}} e^{-\frac{(\tau - t)^2 f^2}{2}} e^{-i2\pi f t} dt \tag{4}$$

TABLE 3. Magnitude of Features Used for DT Rules.

PQ Disturbance	Class Symbol	Features of PQ Events						
		F1	F2	F3	F4	F5	F6	F7
Sag + harmonics	C1	-0.1461	3.3652×10^{-14}	0.7133	1.4925	1.4631	5.5034	59.5543
Swell + harmonics	C2	12.9355	-5.3517×10^{-15}	1.2882	1.4885	2.1228	2.5602	57.1187
Interruption + harmonics	C3	8.7609	-0.0442	0.1112	1.4792	1.9245	1.6948	53.7258
Flicker + harmonics	C4	16.9196	4.738410^{-06}	1.0008	2.8443	1.6005	1.8120	55.8628
Sag + OT	C5	52.7236	-3.2150	1.1971	9.1370	11.37777	11.6667	5.9238
Swell + OT	C6	54.5176	-5.1062	1.3360	5.3525	27.1077	11.2492	5.7132
Flicker + OT	C7	55.6577	-3.7059	1.6713	20.4860	14.7995	11.0207	6.0168
Harmonics + OT	C8	54.7945	-4.5339	1.6613	18.3052	21.6510	11.5610	6.0045
Sag + IT	C9	72.8867	-0.8836	0.8685	1.4193	2.5287	55.4795	11.1341
Swell + IT	C10	74.5266	-0.7177	1.1519	1.5361	2.3874	53.4223	20.7854
Flicker + IT	C11	69.4366	0.2879	1.1267	2.6787	1.8527	50.2566	13.6665
Harmonics + IT	C12	71.7273	0.2899	1.1275	2.6868	1.8537	1.8537	14.3775
Sag+spike	C13	15.1804	0.0449	0.7286	1.4927	1.4619	6.5109	52.4710
Sag + notch	C14	15.4056	0.0470	0.6666	1.4926	1.4605	3.0241	50.6233
Sag + OT + harmonics	C15	57.4147	-3.6215	1.2059	9.2670	14.5724	13.5146	5.840
Swell + OT + harmonics	C16	65.2167	-5.0823	1.3543	4.8005	26.9323	13.0812	5.6366
Flicker + harmonics + IT	C17	72.6536	0.2900	1.1275	2.6868	1.8537	60.8051	12.2361
Sag + OT + harmonics + IT	C18	135.3815	-4.0078	1.1874	11.4521	18.5164	24.6528	5.809

Width of GW depends on frequency and given as

$$\sigma(f) = T = \frac{k}{|f|} \tag{5}$$

Here T: time period. Considering constant k as unity makes GW narrowest in time domain.

Discrete form of ST is computed by considering advantages of fast Fourier transform (FFT) and convolution theorem. PQ signal h(t) is sampled in to a discrete time series $h(kT)$, considering the sampling time period equal to T and $k = 0, 1, \ldots, N-1$. Discrete form of the Fourier transform (FT) is given by the following relation.

$$H\left[\frac{n}{NT}\right] = \frac{1}{N}\sum_{k=0}^{N-1} h[kT]e^{-\frac{i2\pi nk}{N}} \tag{6}$$

Here, $n = 0, 1, \ldots, N-1$. Discrete ST is considered as projection of vector of time series h[kt] on the set of vectors (spanning). Elements of ST are not independent and vectors (spanning) are not orthogonal. Every base vector of FT is composed of N localized vectors which can be computed by product of N shifted Gaussian. Summation of such N localized vectors is considered as original base vector [33]. ST of a discrete time series $h[kT]$ for $n \neq 0$ is computed by the following relation (considering $f \rightarrow n/NT$ and $\tau \rightarrow jT$) [10].

$$S\left[jT, \frac{n}{NT}\right] = \sum_{m=0}^{N-1} H\left[\frac{m+n}{NT}\right] e^{-\frac{2\pi^2 m^2}{n^2}} e^{\frac{i2\pi mj}{N}} \tag{7}$$

If voice $n = 0$, it is computed and defined as below.

$$S[jT, 0] = \frac{1}{N}\sum_{m=0}^{N-1} h\left[\frac{m}{NT}\right] \tag{8}$$

here j, m, and $n = 0, 1, \ldots, N-1$. ST output is obtained in the form of a complex matrix having size $n \times m$ and designated as S-matrix. This matrix can be represented by below mentioned mathematical formulation.

$$S(\tau, f) = A(\tau, f)e^{-i\varphi(\tau,f)} \tag{9}$$

Here, $A(\tau, f)$: magnitude of amplitude, $\varphi(\tau, f)$: phase. Row and column of ST matrix correspond to frequency and time in respective order. Every column indicates frequency components of the signal at a moment of time. Every row indicates magnitude of a frequency component in respect to time which is indicated by samples ranging from 0 to $N-1$. The S-matrix is used to compute the information related to magnitude, frequency and phase of a signal. Contour of magnitude represents a locus of maximum value computed from ST matrix at a time moment. For computing phase, regions of highest amplitude are examined from S-matrix, and respective phase is computed at these points. Frequencies of signal are computed from ST matrix and detailed by a contour known as frequency contour [30]. ST-amplitude (STA) matrix is utilized for analysis of complex PQ events and computed using equation (7) as $|S[jT, n/NT]|$ whereas the phase can be detailed below.

$$\varphi = tan^{-1}\left\{\frac{imag(S[jT, \frac{n}{NT}])}{real(S[jT, \frac{n}{NT}])}\right\} \tag{10}$$

IV. S-TRANSFORM SUPPORTED ANALYSIS OF COMPLEX PQ EVENTS

The PQ events with complex nature are analyzed with the help of various ST curves computed from S-matrix of Stockwell transform. ST plots used for the analysis include contour of time and frequency (S-contour), amplitude-time plot, phase contour and amplitude-frequency plot. A summing absolute magnitude plot is proposed in addition of above

detailed contours/plots which helps in improving the classification efficiency. The plot is computed by summation of absolute magnitude of every column of ST-matrix. The plots are further utilized to extract various features of the signals. The plots associated with sinusoidal waveform without any disturbance will be considered as reference plots and help in detecting the PQ events. The complex PQ events are grouped as per their order of complexity and their analysis is presented in the following subsections.

A. SECOND ORDER COMPLEX PQ DISTURBANCE

In this subsection, two single stage PQ disturbances are combined in order to generate second order complex PQ disturbances. These disturbances are analysed using multi-resolution analysis supported by S-transform. Various second order complex PQ disturbances considered for analysis are sag in voltage with harmonics, swell in voltage with harmonics, MI with harmonics, flicker with harmonics, sag in voltage combined with OT, swell in voltage with IT, flicker with OT, harmonics with OT, sag in voltage with IT, swell in voltage with IT, flicker with IT, harmonics with IT, sag in voltage with spike and sag in voltage with notch.

1) VOLTAGE SAG WITH HARMONICS

Fig. 2 shows the ST supported plots for sag in voltage with harmonics. Sag in voltage (0.06 *s* to 0.14 *s*) has easily been identified by decreased value of amplitude plot and summing absolute magnitude plot detailed in respective order in Fig. 2(c) and (d). Discontinuity in upper contour of Fig. 2(b) is also an indication of voltage sag. Harmonics can be identified by ripples of continuous nature associated with S-contour and summing absolute magnitude plot detailed in Fig. 2,(b) and (d) in respective order. Frequency contents, in addition to fundamental, detected with finite magnitude between normalized frequencies of 0.05 to 0.15 in amplitude-frequency plot illustrated in Fig. 2 (f) also indicate availability of harmonics with the signal.

To investigate the effect of noise on performance of the algorithm during PQ identification stage, a noise of 20dB SNR is superimposed on the voltage signal with sag and harmonics. Fig. 3 shows the ST supported plots for sag in voltage with harmonics in the presence of 20dB SNR noise level. Sag in voltage (0.06 *s* to 0.14 *s*) has easily been identified by decreased value of amplitude plot and summing absolute magnitude plot detailed in respective order in Fig. 3(c) and (d). Discontinuity in upper contour of Fig. 3(b) is also an indication of voltage sag. Harmonics can be identified by ripples of continuous nature associated with S-contour and summing absolute magnitude plot detailed in Fig. 3(b) and (d) in respective order. Further, presence of noise is also detected by the increased magnitude of ripples on surface of the summing absolute values plot of Fig. 3(d). Frequency contents, in addition to fundamental, identified by finite magnitude between normalized frequencies of 0.05 to 0.15 in amplitude-frequency plot of Fig. 3 (f) also indicate availability of harmonics with the signal. Further, the finite values of the amplitude-frequency plot beyond the normalized frequency of 0.15 indicate the presence of noise. Hence, the proposed algorithm is effective to identify the voltage sag with harmonics even in the presence of noise. Further, noise is also recognized by the summing absolute values plot and amplitude-frequency plot.

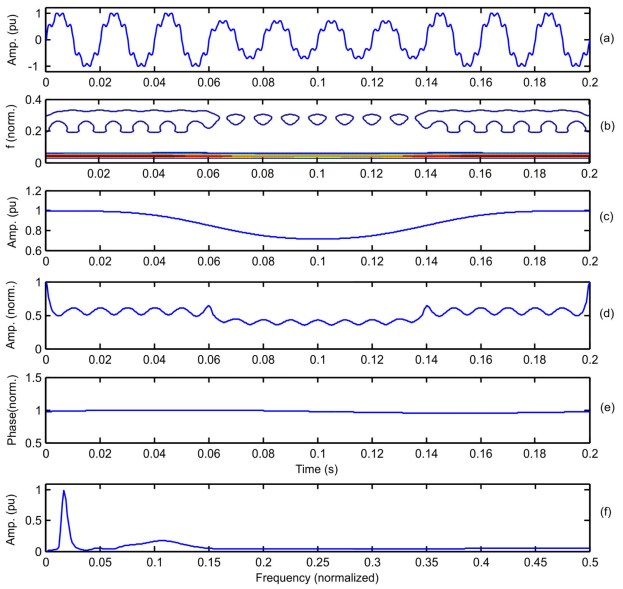

FIGURE 2. (a) Voltage sag with harmonics (b) contour of frequency (c) amplitude plot (d) summing absolute magnitude plot (e) phase plot (f) amplitude-frequency plot.

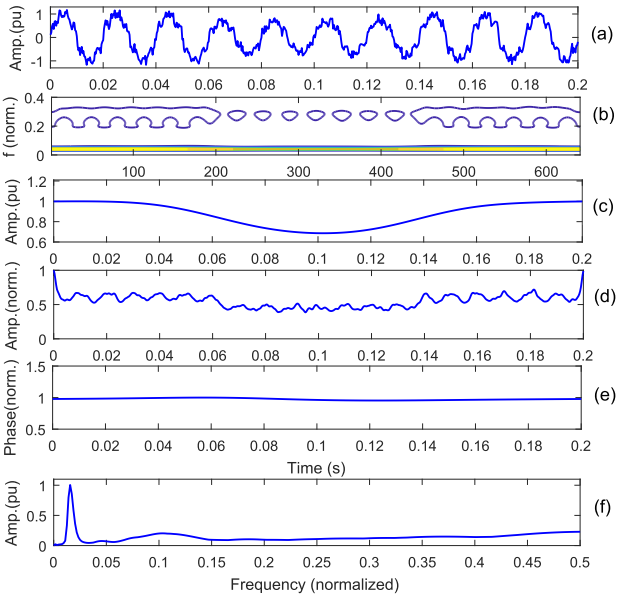

FIGURE 3. Effect of 20dB SNR noise level (a) voltage sag with harmonics and superimposed noise of 20dB SNR (b) contour of frequency (c) amplitude plot (d) summing absolute magnitude plot (e) phase plot (f) amplitude-frequency plot.

2) SWELL IN VOLTAGE WITH HARMONICS

Swell in voltage with harmonics and respective ST supported plots are detailed in Fig. 4. The swell in voltage is identified by increased magnitude of lower S-contour, amplitude curve and summing absolute magnitude plot as detailed in Fig. 4 (b), (c) and (d) in respective order. Harmonics can be recognized by the continuous ripples incident on upper S-contour and summing absolute magnitude plot of Fig. 4 (b) and (d) in respective order. Frequency contents observed in addition to the fundamental and having definite finite magnitude between frequencies (normalized) 0.05 to 0.15 in amplitude-frequency plot detailed in Fig. 4 (f) also indicate availability of harmonics contents with the signal.

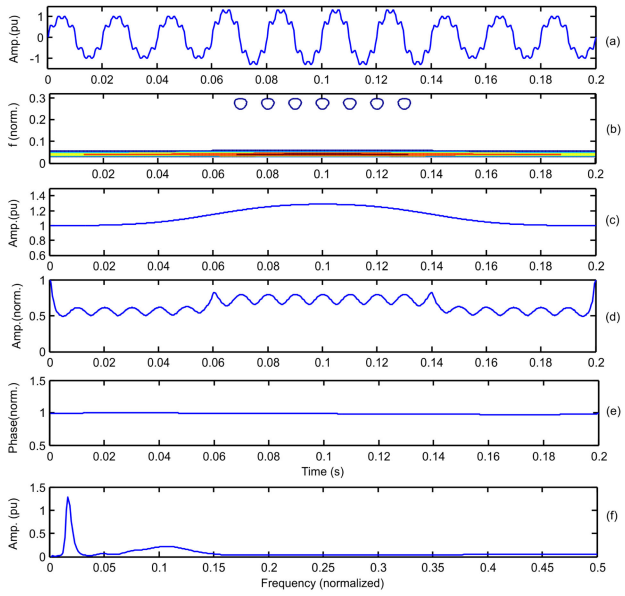

FIGURE 4. (a) Voltage swell with harmonics (b) contour of frequency (c) amplitude plot (d) summing absolute magnitude plot (e) phase plot (f) amplitude-frequency plot.

3) FLICKER WITH HARMONICS

Flicker with harmonics and associated ST supported plots are detailed in Fig. 5. Flicker is recognized by the circles in a series (at the top) in contour of ST as described in Fig. 5 (b) whereas availability of harmonics is recognized by ripples of continuous nature in middle ST-contour. Flicker and harmonics are also observed in summing absolute magnitude plot in the form of continuous ripples as described in Fig. 5 (d). Components of frequency present, in addition to fundamental, and having finite magnitudes between frequencies (normalized) 0.05 to 0.15 in amplitude-frequency plot as described in Fig. 5 (f) show the availability of harmonics associated with signal whereas the finite magnitude in between frequencies (normalized) 0.2 to 0.3 represents the flicker in signal. However, amplitude and phase curves give no information about the flicker and harmonics.

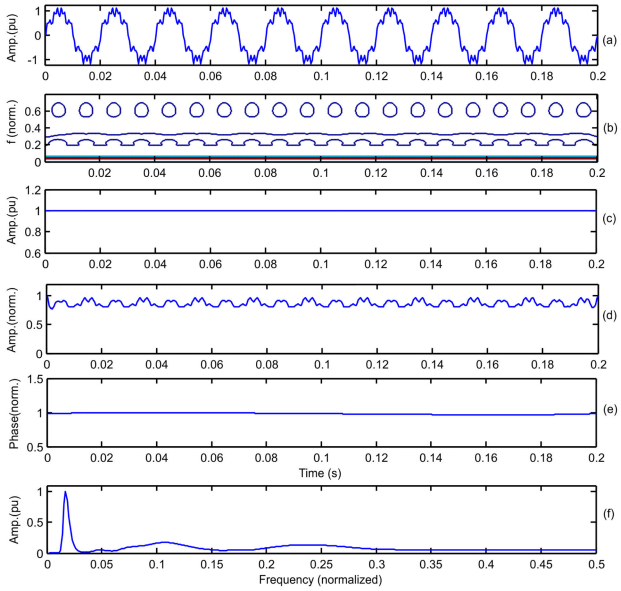

FIGURE 5. (a) Flicker with harmonics (b) contour of frequency (c) amplitude plot (d) summing absolute magnitude plot (e) phase plot (f) amplitude-frequency plot.

4) SAG IN VOLTAGE WITH OT

Simultaneous occurrence of voltage sag with oscillatory transient (OT) and associated ST supported plots are detailed in Fig. 6. Sag in voltage (0.06 *s* to 0.14 *s*) is identified easily by decreased magnitude in amplitude and summing absolute magnitude plot of Fig. 6 (c) and (d) in respective order. Decrease in magnitude (0.06 *s* to 0.14 *s*) in contour of ST detailed in Fig. 6 (b) also indicates availability of sag in voltage. Presence of the OT is identified by an isolated single contour (0.09 *s* to 0.11 *s*) as described in Fig. 6 (b). Availability of OT is also identified by changes which are significant between 0.09 *s* to 0.11 *s*, in all plots of Fig. 6. Frequency contents identified, in addition to fundamental, having finite values between frequencies (normalized) 0.05 to 0.25 in amplitude-frequency plot as detailed in Fig. 6(f) also indicate availability of OT in the signal.

5) FLICKER WITH OSCILLATORY TRANSIENT

Flicker with OT and associated ST supported plots are detailed in Fig. 7. Presence of OT is identified by isolated single contour (0.08 *s* to 0.10 *s*) as detailed in Fig. 7 (b). Availability of OT is also recognized by significant changes, in between 0.08 *s* to 0.10 *s*, in all ST supported curves detailed in Fig. 7. Frequency contents other than the fundamental seen with finite magnitude, in between frequencies (normalized) 0.05 to 0.25, as detailed in Fig. 7 (f) also indicate the availability of OT in the signal. Flicker is detected by sustained ripples in summing absolute magnitude plot of Fig. 7 (d). This is also recognized by upper surface of isolated ST contour of Fig. 7 (b) in the form of ripples.

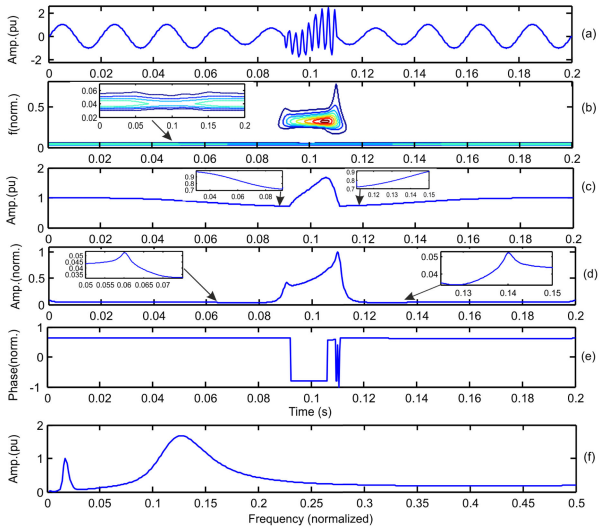

FIGURE 6. (a) Voltage sag with OT (b) contour of frequency (c) amplitude plot (d) summing absolute magnitude plot (e) phase plot (f) amplitude-frequency curves.

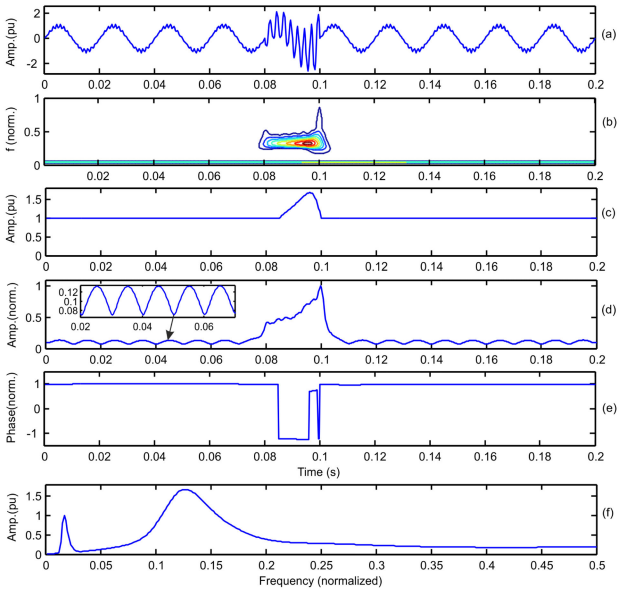

FIGURE 7. (a) Flicker with oscillatory transient (b) contour of frequency (c) amplitude plot (d) summing absolute magnitude plot (e) phase plot (f) amplitude-frequency plot.

6) SAG IN VOLTAGE WITH IT

Sag in voltage with IT and associated ST supported plots are described in Fig. 8. Sag in voltage (0.06 *s* to 0.14 *s*) can be recognized by decreased magnitude of amplitude and summing absolute magnitude plots of Fig. 8 (c) and (d) in respective order. Voltage sag is also detected in ST contour of Fig. 8 (b) by decrease in magnitude. Availability of the impulsive magnitude in both the ST contour and summing absolute magnitude plots as detailed in Fig. 8 (b) and (d) indicate the IT associated with the signal. As IT has all frequencies, hence frequency-amplitude plot has finite values throughout the range of frequency as detailed in Fig. 8 (f).

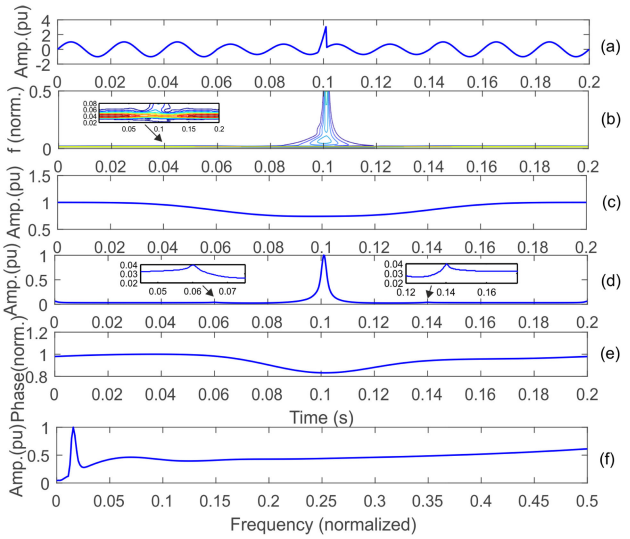

FIGURE 8. (a) Voltage sag with IT (b) contour of frequency (c) amplitude plot (d) summing absolute magnitude plot (e) phase plot (f) amplitude-frequency plot.

7) FLICKER WITH IT

The flicker with IT having high magnitude compared to the signal magnitude and associated S-transform based curves are described in Fig. 9. Availability of flicker is recognized by circles incident in the form of a series in contour of ST as illustrated in Fig. 9 (b). Flicker is also detected by sustained ripples in summing absolute magnitude plot as described in Fig. 9 (d). Impulsive magnitude observed in both the contour of ST and summing absolute magnitude plot as detailed in Fig. 9 (b) and (d) in respective order indicates IT associated with the signal. Continuous finite values as described in Fig. 9 (f) also indicate availability of the IT associated with the signal. The flicker with IT having magnitude comparable to the signal magnitude and associated S-transform based curves are described in Fig. 10. It is observed that these plots are effective to recognize the flicker with IT having magnitude comparable to signal magnitude in the similar way as discussed above. Hence, method is effective to identify the flicker with IT of all magnitude.

Effect of 20 *dB* SNR noise on performance of the algorithm is investigated to identify the flicker with IT. The flicker with IT and associated S-transform based curves in the presence of 20 *dB* SNR noise are described in Fig. 11. Availability of flicker is recognized by circles incident in the form of a series in contour of ST as illustrated in Fig. 11 (b). Flicker is also detected by sustained ripples in summing absolute magnitude plot as described in Fig. 11 (d). Further, presence of the noise is also detected by the increased magnitude of ripples on surface of the summing absolute values plot of Fig. 11 (d). Impulsive magnitude observed in both the contour of ST and summing absolute magnitude plot as detailed in Fig. 11 (b) and (d) in respective order indicates IT associated with the signal. Continuous finite values as described in Fig. 11 (f) also indicate availability of the IT associated with the signal. Further, the finite values of the

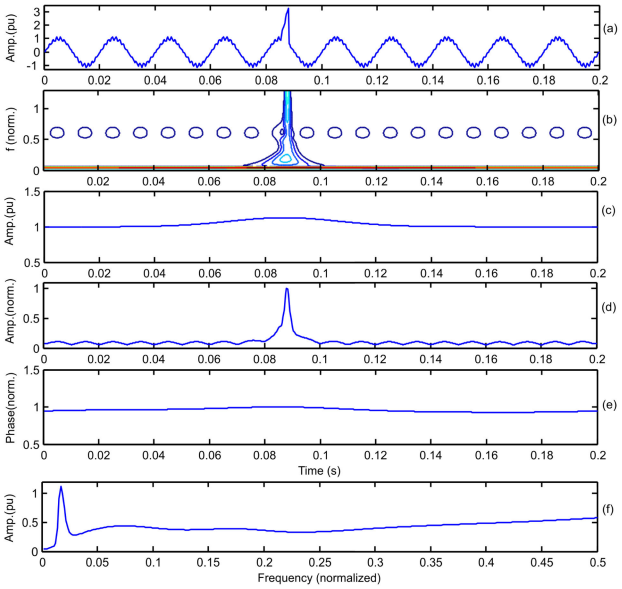

FIGURE 9. (a) Flicker with IT having high magnitude compared to the signal magnitude (b) contour of frequency (c) amplitude plot (d) summing absolute magnitude plot (e) phase plot (f) amplitude-frequency plot.

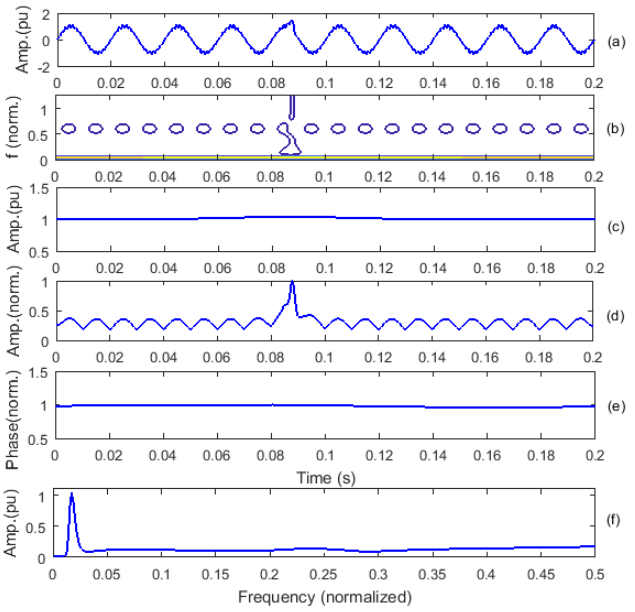

FIGURE 10. (a) Flicker with IT having magnitude comparable to the signal magnitude (b) contour of frequency (c) amplitude plot (d) summing absolute magnitude plot (e) phase plot (f) amplitude-frequency plot.

amplitude-frequency plot beyond the normalized frequency of 0.25 indicate the presence of noise. Hence, the proposed algorithm is effective to identify the flicker with IT even in the presence of noise. Further, noise is also recognized by the summing absolute values plot and amplitude-frequency plot.

8) SAG IN VOLTAGE WITH MULTIPLE SPIKES

Simultaneous incidence of sag in voltage with multiple spikes and associated ST supported plots are detailed in Fig. 12. Sag in voltage (0.06 *s* to 0.14 *s*) can be identified by reduced

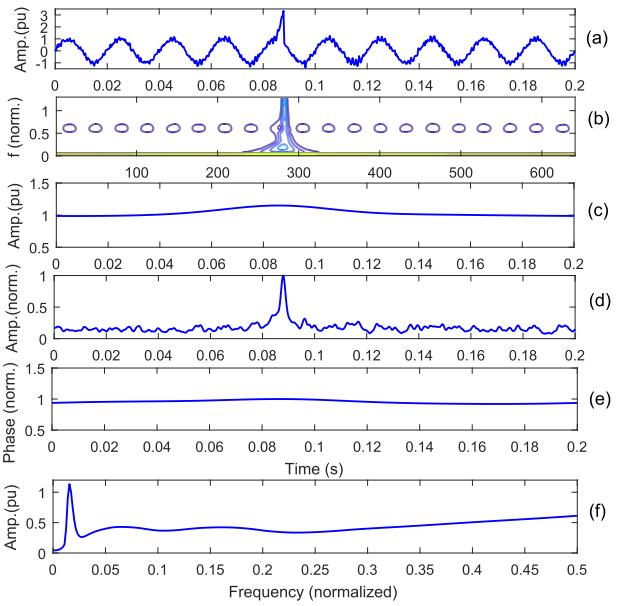

FIGURE 11. Effect of 20dB SNR noise level (a) Flicker with IT and superimposed 20dB SNR noise (b) contour of frequency (c) amplitude plot (d) summing absolute magnitude plot (e) phase plot (f) amplitude-frequency plot.

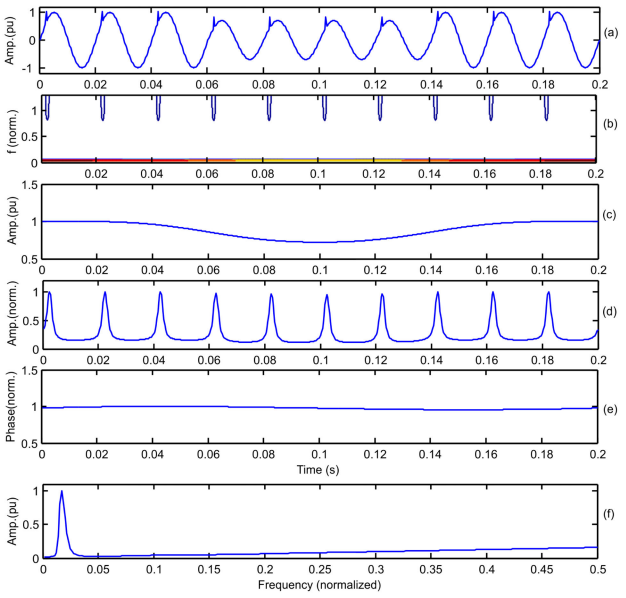

FIGURE 12. (a) Voltage sag with multiple spikes (b) contour of frequency (c) amplitude plot (d) summing absolute magnitude plot (e) phase plot (f) amplitude-frequency plot.

magnitude of amplitude plot of Fig. 12 (c). Multiple spikes can easily be identified by contours in a series associated with ST-contour and ripples of continuous nature in summing absolute magnitude plot as described in Fig. 12(b) and (d) in respective order.

B. THIRD ORDER COMPLEX PQ DISTURBANCES

Three single stage PQ disturbances are combined in order to obtain third order complex PQ disturbances and analysed

using multi-resolution analysis supported by S-transform. Various third order complex PQ disturbances considered for the analysis include sag in voltage with OT and harmonics, swell in voltage with OT and harmonics, flicker with IT and harmonics. Results related to detection of the flicker with harmonics and IT is discussed in this section.

ST supported plots of flicker with harmonics and IT are described in Fig. 13. Harmonics are identified by ripples of sustained nature associated with middle S-contour as detailed in Fig. 13 (b). Availability of flicker is recognized by circles present in the form of a series associated with upper ST-contour as detailed in Fig. 13 (b). Sustained ripples available in summing absolute magnitude plot as illustrated in Fig. 13 (d) are because of combined impact of flicker and harmonics in the signal. Impulsive magnitude seen in both the ST-contour and summing absolute magnitude plot as detailed in Fig. 13 (b) and (d) in respective order indicates IT associated with the signal. Continuous finite values as described in Fig. 13 (f) also indicate availability of the IT. Phase magnitude also increases at the time of IT associated with the signal.

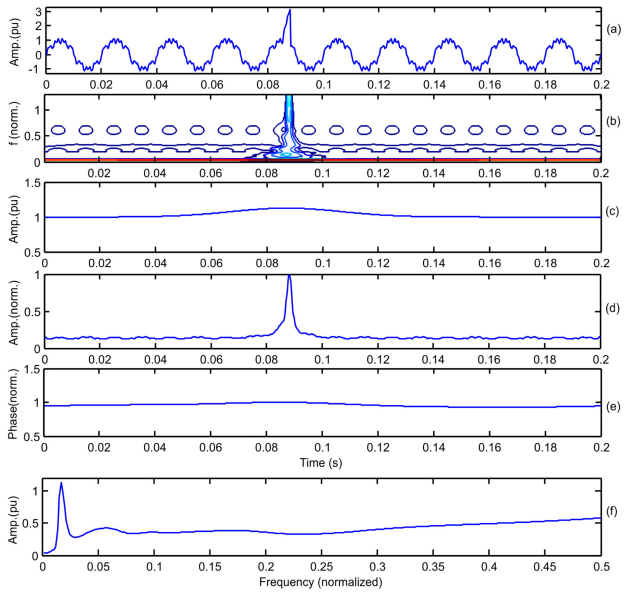

FIGURE 13. (a) Flicker with harmonics and IT (b) contour of frequency (c) amplitude plot (d) summing absolute magnitude plot (e) phase plot (f) amplitude-frequency plot.

C. FOURTH ORDER COMPLEX PQ DISTURBANCE

In this subsection, ST supported analysis of fourth order complex PQ disturbance is presented. Disturbance is obtained by the combination of four single stage PQ disturbances. Results related to detection of the sag in voltage with OT, Harmonics and IT is discussed in this section.

Signal of voltage with OT, sag in voltage, harmonics and IT is illustrated in Fig. 14. Sag in voltage (0.06 *s* to 0.14 *s*) can be recognized by reduced magnitude of amplitude plot of Fig. 14 (c). Harmonics can be recognized by ripples of sustained nature in summing absolute magnitude plot as

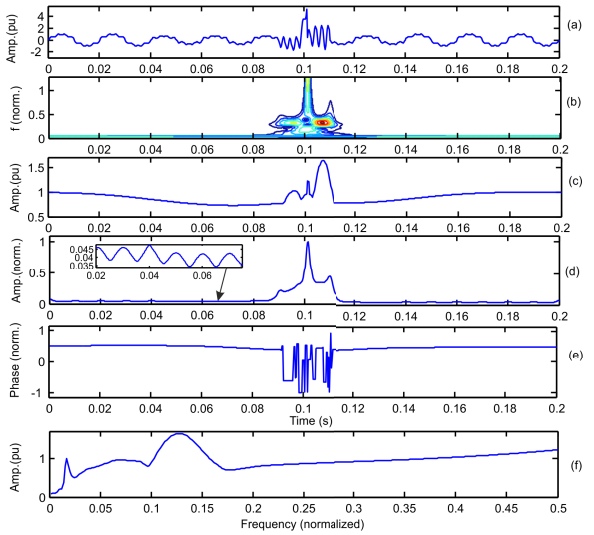

FIGURE 14. (a) Voltage sag with OT, IT and harmonics (b) contour of frequency (c) amplitude plot (d) summing absolute magnitude plot (e) phase plot (f) amplitude-frequency plot.

detailed in Fig. 14 (d). Significant changes between 0.09 *s* to 0.11 *s* in all plots of Fig. 14 are due to combination of IT with the OT. The sharp peak available in curves of Fig. 14 (b), (c) and (d) for the duration 0.098 *s* to 0.101 *s* indicate availability of IT while high magnitude of these curves in between 0.09 *s* to 0.11 *s* identify availability of the OT. Peak, in addition to fundamental frequency, recognized with finite magnitude in between the frequencies (normalized) 0.01 to 0.18 as detailed in Fig. 14 (f) also gives an indication of OT in the signal. Increased magnitude of frequency plot described in Fig. 14 (f) also recognizes the IT associated with the signal.

Therefore, it is concluded that their is various similarities as well as dissimilarities in ST supported plots of different multiple PQ events. Thus, there is a requirement for introducing additional features which can be computed using the statistical approaches for classification of the PQ events of complex nature.

V. S-TRANSFORM SUPPORTED FEATURES OF COMPLEX PQ EVENTS

Different features of statistical nature computed from ST supported plots of PQ events of complex nature are labelled as F1 to F7. Description of these features is provided below.

F1: Summing factor $Sf = max(S) + min(S) - max(R) - min(R)$, here S is an array of data for summing absolute magnitudes of a signal of complex PQ event and R is an array of data for summing of absolute magnitudes of pure sine wave (reference). Zero magnitude of this factor recognizes that there is no disturbance associated with the signal whereas finite magnitude indicates the presence of PQ disturbance.

F2: Skewness computed from phase plot. Skewness can be computed using the following relation.

$$s = \frac{E(x-\mu)^3}{\sigma^3} \tag{11}$$

Here, x: signal data array, μ: mean of signal x, σ: standard deviation of signal x, and E: expected magnitude of quantity.

F3: Amplitude factor $Af = (1 + (C - A) + (D - B))$, here C: maximum magnitude of amplitude plot of arbitrary signal, D: minimum magnitude of amplitude plot of arbitrary signal, A: maximum magnitude of amplitude plot of pure sine wave (considered as reference signal) and B: minimum magnitude of amplitude curve of pure sine wave.

F4: Kurtosis computed from amplitude plot. Kurtosis (k) of a signal can be computed by the following relation.

$$k = \frac{E(x - \mu)^4}{\sigma^4} \tag{12}$$

Here, x: signal data array, μ: mean of signal x, σ: standard deviation of signal x, and E: expected magnitude of quantity.

F5: Kurtosis computed from phase plot. Equation (12) is used to calculate the feature F5 where x indicates data array of phase curve obtained by S-transform based decomposition of signal with PQ disturbance. Here, μ represents the mean of x, σ represents standard deviation of x, and E is expected magnitude of quantity.

F6: Kurtosis computed from the summing absolute magnitude plot. Equation (12) is used to calculate the feature F6 where x indicates data array of summing absolute magnitude plot obtained by S-transform based decomposition of signal with PQ disturbance. Here, μ represents the mean of x, σ represents standard deviation of x, and E is expected magnitude of quantity.

F7: Kurtosis of amplitude-frequency curve. Equation (12) is used to calculate the feature F7 where x indicates data array of amplitude-frequency curve obtained by S-transform based decomposition of signal with PQ disturbance. Here, μ represents the mean of x, σ represents standard deviation of x, and E is expected magnitude of quantity.

Accuracy of the algorithm depends on selection of the features. Large number of features may give better accuracy of the algorithm but implementation time increases due to handling of large number of data of the various features. The system becomes more complex and slow in detection of the PQ disturbances due to the handling of large data. Further, large storage capacity will be required to handle large data. This will also increase the cost of device. The proposed algorithm uses only 7 features against the method proposed in [24] which uses 14 features. The additional 7 features used in [24] include peaks associated with ST supported frequency-amplitude curve, standard deviation of S-matrix, variance of S-matrix (amplitude), energy content of S-contour, maximum deviation computed from S-matrix (amplitude), and second order derivative of summing absolute magnitude plot. Proposed study has eliminated the requirement of S-contour and second order derivative of summing absolute magnitude plot. Hence, proposed algorithm needs minimum number of features in comparison to technique reported in [24]. Study presented in this article and paper [24] has been performed using same mathematical formulation of PQ events in accordance with IEEE-1159 standard. Studies in both of these papers have been performed using MATLAB 2015b software.

VI. CLASSIFICATION OF COMPLEX PQ EVENTS USING RULE-BASED DT

The introduced algorithm makes use of features F1 to F7 to design the rules for classifying the complex PQ disturbances. Numerical values of features computed using the relations discussed in the Section V and used to design rules is presented in Table 3. Variance in these values increases the computational time which is 17.1509 *ms* for this set of values. These features take care of the different characteristics of the complex PQ disturbances and deviation of the waveform from the pure sinusoidal nature. Hence, these features can be effectively used to identify the type of complex PQ disturbance. Threshold values of the features (F2-F7) used for classification of the complex PQ disturbances using RBDT have been decided by testing the proposed algorithm on 100 data sets of each complex PQ disturbance obtained by changing the parameters including amplitude of signal from standard value of 1 per unit, time of incidence of complex PQ disturbance, harmonic frequencies, time of initiation and end of PQ disturbance, amplitude and frequency of transients, frequency of voltage signal (50 Hz and 60 Hz) and different levels of noise [refer Appendix]. Further, that particular value of threshold is selected for a feature which helps to effectively identify all the complex PQ disturbances.

Presence of PQ disturbance is identified by the non-zero values of feature F1. This feature has zero value for pure sine wave of voltage signal without PQ disturbance. The other features (F2 to F7) are fed to rule based DT for further classification. The signals are initially classified in the categories G1 and G2 based on kurtosis of phase curve (F5). Data of category G1 contains signals with F5>6 whereas data category G2 pertains to signals with F5<6. The group G1 includes the signals with PQ disturbances which contains the OT whereas the group G2 includes the disturbances without OT.

Signals categorized under category G1 are categorized in subcategories G11 and G12 supported by magnitude of kurtosis of amplitude curves (F4). Category G11 includes the signals with F4<14 and signals with F4>14 are categorized under category G12. Two signals in the category G12 are subsequently categorized using magnitude of kurtosis of phase curve (F5). The OT with harmonics (C8) will have F5> 18 whereas the OT with flicker (C7) will have F5< 18. Voltage sag with harmonics, OT and IT (C18) will have kurtosis of summing absolute magnitude plot (F6)> 18. All other signals of group G11 will have F6<18 and classified under group G111. Signals in the group G111 are further categorized into groups G112 and G113 supported by magnitude of kurtosis of phase curve (F5). Signals under group G113 will have F5>18 whereas the signals related to group G112 will have F5<18. Two signals in the category G113 are subsequently categorized based on magnitude of sum factor (F1). Voltage swell with OT (C6) will have F1<60 whereas voltage swell with OT and harmonics (C16) will have F1>60. Two signals

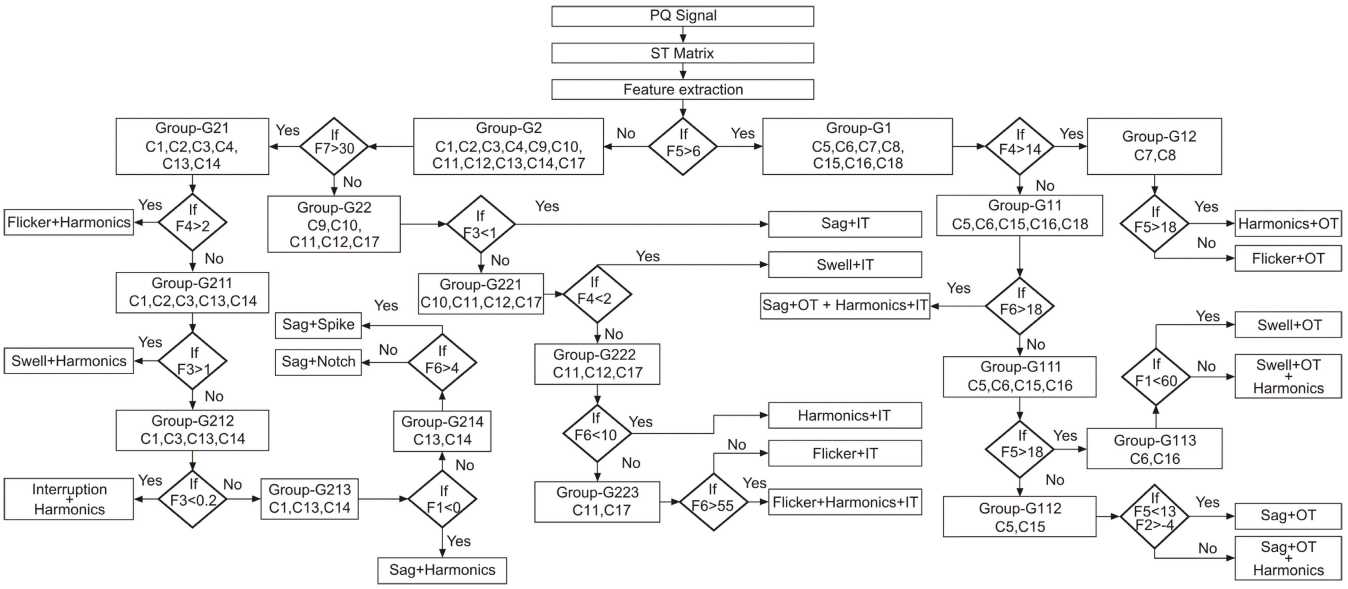

FIGURE 15. Rule-based DT methodology to classify multiple PQ events.

included in the group G112 are further discriminated from each other based on the values of kurtosis of phase curve (F5) and skewness of phase curve (F2). Voltage sag with OT (C5) will have F2> -4 and F5<13 whereas the voltage sag with OT and harmonics (C15) will have F2<-4 and F5>13.

Signals included in group G2 are categorized into subcategories G21 and G22 using magnitude of kurtosis of amplitude-frequency curve (F7). Signals under group G21 will have F7> 30 whereas the signals related to group G22 will have F7< 30. The PQ disturbances classified under group G22 contains the IT whereas the group G21 contains the signal without IT. PQ disturbances included in the group G21 are discriminated from each other based on the different features. Flicker with harmonics (C4) will have F4>2. All other signals of group G21 will have F4<2 and are included in the group G211. Voltage swell with harmonics (C2) is discriminated based on the value of amplitude factor (F3). This will have F3> 1 whereas all other signals included in the group G211 will have F3<1 and are classified under the group G212. Voltage interruption with harmonics (C3) will have F3< 0.2. All other signal related to group G212 will have 0.2< F3<1 and are classified under the group G213. Voltage sag with harmonics (C1) has been discriminated from the signals of group G213 based on the values of sum factor (F1). The signal C1 will have F1< 0 and all other signals are categorized in group G214. Two signals in the group G214 are subsequently categorized using magnitude of kurtosis of summing absolute magnitude plot (F6). Voltage sag with spike (C13) will have F6> 4 whereas the voltage sag with notch (C14) will have F6< 4.

Signals considered in the category G22 are subsequently categorized in the subcategories G221 and voltage sag with IT (C9) based on the value of amplitude factor (F3). The signals under group G221 have F3>1 and signal C9 have F3<1. Signals included in category G221 are differentiated one by one using various features. Voltage swell with IT (C10) will have F4<2 whereas all other signals of group G221 will have F4> 2 and are classified under the group G222. Harmonics with IT (C12) will have F6<10 whereas other signals included in the group G222 will have F6> 10 and are categorized in category G223. Two signals included in category G223 are categorized using magnitude of F6. Flicker with IT (C11) will have F6<55 whereas the flicker with IT and harmonics (C17) will have F6>55. The rule-based DT algorithm for categorization of the complex PQ events is illustrated in Fig. 15.

Efficiency of proposed algorithm is established in terms of effectively classified and misclassified signals supported by testing for 30 sets of data for each event. Gaussian noise of level 20 dB SNR is superimposed on signals to evaluate performance in noisy environment using MATLAB command *awgn*. This noise level is selected because noise level higher than 20 dB SNR is not observed in the practical power system applications [24]. The noise level of 10dB SNR is normally associated with the communication systems and not with the power system. Hence, this algorithm has not been tested for 10 dB SNR noise level. Table 4, represents the performance of proposed method to classify the different signals in the absence of noise and presence of 20 *dB* SNR. It is observed that the classification efficiency of the algorithm is 98.70% in the absence of noise and 97.41% in the presence of noise level of 20 *dB* SNR. It is also established that in the presence of noise levels of 40 *dB* SNR, 60 *dB* SNR, and 80 *dB* SNR, the classification accuracy is found to be 97.67%, 97.99%, 98.28%, and 98.57% respectively.

TABLE 4. Classification Results of Complex PQ Disturbances.

PQ event	Correctly classified		Misclassified		Accuracy (%)	
	without noise	20 dB SNR	without noise	20 dB SNR	without noise	20 dB SNR
C1	30	30	0	0	100	100
C2	30	30	0	0	100	100
C3	30	30	0	0	100	100
C4	30	29	0	1	100	96.67
C5	30	30	0	0	100	100
C6	30	30	0	0	100	100
C7	30	29	0	1	100	96.67
C8	29	29	1	1	96.67	96.67
C9	30	30	0	0	100	100
C10	30	30	0	0	100	100
C11	30	29	0	1	100	96.67
C12	30	30	0	0	100	100
C13	29	29	1	1	96.67	96.67
C14	29	29	1	1	96.67	96.67
C15	30	29	0	1	100	96.67
C16	29	28	1	2	96.67	93.33
C17	28	27	2	3	93.33	90.00
C18	29	28	1	2	96.67	93.33
Overall accuracy: 98.70% (without noise), 97.41% (with 20 dB SNR)						

The proposed ST supported DT method identified and classified the investigated PQ disturbances in time duration of 17.1509 *ms*. This is achieved due to the use of minimum (seven) effective features which decreased the implementation time due to reduced data handling requirement. This makes the algorithm less complex, fast, and reduced requirement of storage.

VII. RESULT VALIDATION IN REAL TIME

Results are validated in real time using a RTDS of OPAL-RT. Results computed in real time using the experimental set-ups of RTDS illustrated in Fig. 16 are comparable to the results computed using simulation. A laptop used as human interface device (HID) has configuration of 64-bit operating system, 4 GB RAM, Intel(I) Core(TM)i5-3230M CPU@2.60 GHz processor. This HID interacts with RTDS using ether-net based communication between the laptop computer and RTDS. Mathematical models are used for modelling the complex PQ events in MATLAB/Simulink 2011b scenario on the HID. The signals are then loaded on ML605 target of RTDS for real time simulation in hardware synchronization mode. Data are recorded using OpWrite block of RT-Lab and analysed using ST. Results are validated on 30 sets of data for every PQ event. Performance of proposed technique is evaluated in terms of correct and incorrect classified signals. Gaussian noise of 20 dB SNR is superimposed for computing performance of algorithm in the noisy condition. Real time performance and its comparison with simulated results are presented in Table 5.

VIII. PERFORMANCE COMPARISON

This section details a study to compare the performance of PQ detection and classification approaches. A brief study is also presented to compare the performance of various types of the classifiers for classification of the investigated 18 complex PQ disturbances.

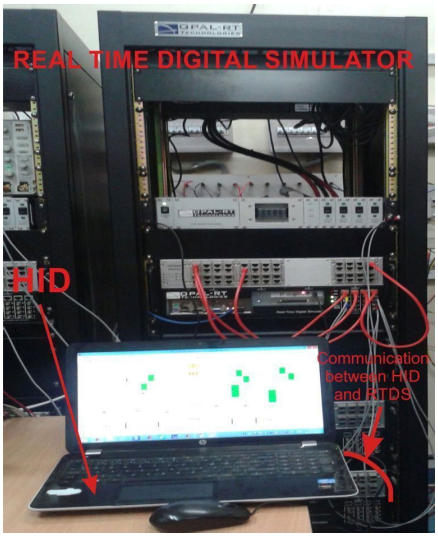

FIGURE 16. Experimental set up for real time results.

A. PERFORMANCE COMPARISON OF THE ALGORITHMS

Accuracy of algorithm is compared with techniques introduced in papers [1], [4], [5], [8], [13] and [14]. These articles are selected due to the fact that multiple PQ events are also considered in these articles. Further, in all these articles the PQ events have been generated in accordance with IEEE-1159 standard with the help of mathematical formulation in MATLAB software. However, hardware validation of results has been performed in [8]. Data related to multiple PQ disturbances reported in these papers are considered for comparison of results for validating effectiveness of method. Further, noise level of 20 dB SNR is considered in all articles used for comparative study. Table 6, details the performance results for different techniques in the presence and absence of noise. It is evident from Table 6 that this algorithm has superior efficiency in comparison to algorithms reported in [1], [4], [5], [8], [13] and [14]. Thus, the algorithm making use of S-transform and DT classifier shows good efficiency of categorization compared to different techniques reported in literature. This article has considered 18 complex PQ disturbances in contrast to the other articles which have considered few complex PQ disturbances along with single stage PQ disturbances. Hence, this manuscript introduced a generalized approach for identification of the complex PQ events. The proposed algorithm used less number of features compared to the [4], [5], [8], and [13] which ensure that data handling requirement is decreased resulting in reduced computational burden. Performance of algorithm for testing the PQ disturbances reported in [24] is greater than 99%. Further, performance of algorithm cannot be compared with that reported in [24] as the algorithm proposed in [24] investigates only single stage PQ disturbances and algorithm proposed in this article investigates the complex PQ events. Complex power quality disturbances have high complexity compared to single stage PQ events. Hence, the techniques used for identification of single stage PQ events have high efficiency compared to that utilized for identification of the

TABLE 5. Comparison of Simulation and Real Time Classification Results.

PQ event	Accuracy (%) (Real time)		Accuracy (%) (simulated)		Percentage deviation	
	without noise	20 dB SNR	without noise	20 dB SNR	without noise	20 dB SNR
C1	100	100	100	100	0	0
C2	100	100	100	100	0	0
C3	100	96.67	100	100	0	3.33
C4	96.67	96.67	100	96.67	3.33	0
C5	100	100	100	100	0	0
C6	100	96.67	100	100	0	3.33
C7	100	96.67	100	96.67	0	0
C8	96.67	96.67	96.67	96.67	0	0
C9	100	100	100	100	0	0
C10	100	100	100	100	0	0
C11	96.67	96.67	100	96.67	3.33	0
C12	100	100	100	100	0	0
C13	96.67	96.67	96.67	96.67	0	0
C14	96.67	93.33	96.67	96.67	0	3.4
C15	100	96.67	100	96.67	0	0
C16	96.67	93.33	96.67	93.33	0	0
C17	93.33	90.00	93.33	90.00	3.33	3.33
C18	96.67	93.33	96.67	93.33	3.4	3.56
Overall accuracy of real time results: 98.33% (without noise), 96.85% (with 20 dB SNR)						

TABLE 6. Performance Comparison.

Reference	Type of technique	Numbers of Complex PQ disturbances investigated	Number of features	Overall accuracy (%)
[1]	ST+APSO	4	6	96.50
[4]	DWT+Wavelet networks	8	8	97.50
[5]	Spline WT+ ST	3	8	97.00
[8]	ADALINE+ FFNN	8	10	90.00
[13]	ST+NN	2	14	96.50
[14]	ST+FES	4	5	94.00
Proposed	ST+DT	18	7	98.70

complex PQ events. However, if same algorithm is applied for recognition of complex PQ events then its accuracy decreases drastically and most of the complex PQ disturbances are not detected by these algorithms.

B. PERFORMANCE COMPARISON OF THE CLASSIFIERS

Performance of the proposed DT based classifier is compared with the performance of OneR, ZeroR and Decision stump classifiers to classify all the investigated 18 types of complex nature PQ events. This is achieved in terms of the percentage of correctly classified PQ disturbances for the 30 data used for testing the algorithm and results are detailed in Table 7. OneR classifier produces one level DT based on set rules and test one attribute. ZeroR is a primitive learning classifier which uses category class and average class values. Description of the OneR and ZeroR is available in [34]. Decision stump is a single split DT which is a weak learner and described in [35]. Performance of the OneR, ZeroR and Decision stump is evaluated using all the features discussed in Section V and averaged value is used for comparative study. It is observed from the table 7 that accuracy of the proposed DT is high compared to the OneR, ZeroR and Decision stump classifiers. Further, the proposed DT is fast compared to the above mentioned classifiers.

TABLE 7. Performance of Classifiers to Classify the Complex PQ Disturbances.

Classifier	Correctly classified disturbances (%)	Time of classification (second)
OneR	78.19%	0.710
ZeroR	66.49%	0.721
Decision stump	71.61%	0.112
Proposed DT	98.70%	0.017

IX. IMPLEMENTATION OF PROPOSED ALGORITHM IN PQ MONITORING DEVICES

The basic working principle of online complex power quality monitoring device based on the proposed algorithm is illustrated in Fig. 17. Following are main steps/stages which will be involved in the design of the device.

- The network parameter monitoring system capture seven inputs at the measurement point using signal cards. Three inputs are used for continuous tracking of the phase voltages, three inputs are used for current in all the phases and one input is used for the neutral voltage. On the modern grid substations, the multi-function meters (MFM) directly receive the voltage and current signals from the current transformer (CT) and potential transformer (PT).
- The signals from the signal cards are given as input to the remote terminal unit (RTU) installed on the feeder panels. The RTU has inbuilt Analog to Digital Converter (ADC) unit. The analog voltage as well as current signals given as input to the RTU unit is converted to corresponding digital signals using ADC.
- Digital form of input signals will be transmitted to digital signal processing (DSP) unit. Proposed algorithm is used to process the input current or voltage signals in this unit to recognize complex PQ events available with signals. The proposed algorithm may be performed as embedded functions in field programmable gate array (FPGA) used as DSP unit. FPGA contains an array of configurable logic blocks (CLBs),

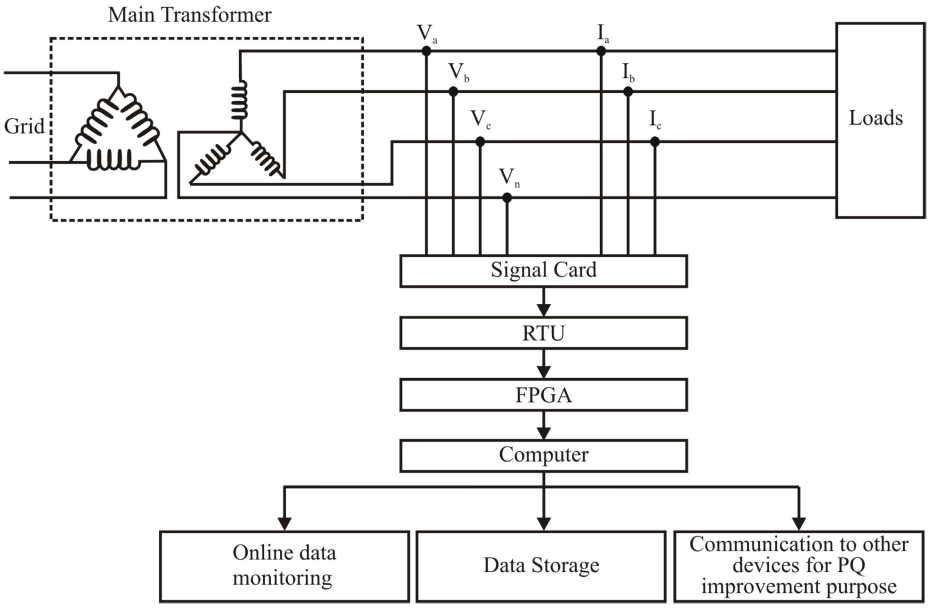

FIGURE 17. Basic working principle of online complex power quality monitoring device based on the proposed algorithm.

memory, DSP slices and additional components. These can be programmed with the help of high-level languages such as VHDL and Verilog. DSP and FPGA are different and cannot replace each other. However, DSP based PQ recognition technique can be implemented with the help of FPGA by the use of DSP slices as one of the component of FPGA.

- The real time complex PQ data obtained by processing the input signals on FPGA units are transmitted to the monitoring centre using transmission control protocol (TCP) or internet protocol (IP). The under datagram protocol (UDP)/IP communication protocol may also be used. The latter is fast compared to former and also allows continuous packet streams for transmission. Hence, the UDP/IP protocol is preferred for monitoring of the complex PQ events.
- In monitoring unit, complex PQ events are monitored continuously using the software on server/client computers. The data of complex PQ disturbances may also be recorded for off-line data analysis or future reference. The complex PQ data may also be communicated to the other devices for initiation of an action for PQ improvement. The improvement of power quality is achieved using distribution static compensator (DSTATCOM) [36], unified PQ conditioner (UPQC) [37], active power filter (APF) [38] etc.
- Design of the PQ monitoring devices will not depend on the order of complexity of the complex PQ events because PQ events are identified based on the patterns and feature values. Procedure for pattern recognition and estimation of features will be same irrespective of the type of PQ disturbance.

X. CONCLUSION

A technique supported by ST and ruled DT has been proposed for recognition of the complex PQ events. Signals are processed using ST based MRA to obtain the ST plots. Features computed from these plots have been used for designing rules for the DT. A new S-transform based plot designated as summing absolute magnitude plot and its features are introduced for achieving high efficiency of identification. Performance of algorithm has been validated using a large set of complex PQ events with and without noise. An efficiency of 98.70% has been achieved without noise. The efficiency of proposed algorithm has been found to be 97.41% with noise level of 20 dB SNR. This algorithm is also tested for noise level ranging from 20 dB SNR to 100 dB SNR and found satisfactory. It is concluded that performance of the proposed ST and DT based approach is superior compared to the FCM & APSO, WT & NN, spline WT & ST, ST & NN, and ST & FES based PQ recognition methods. The simulation results are validated by comparison with results in real time computed by RTDS. Real time results are found to be very close to results of simulation having an error less than 4% which indicates that proposed algorithm is highly effective. The competency of algorithm is established by comparing with the methods reported in literature. The proposed approach is effective for recognizing the wide range of complex PQ events by the use of minimum features. The proposed method proved to have low computational burden and high accuracy of classification even in noisy environment. The important stages in the design of complex PQ monitoring device based on the proposed algorithm are also presented. Thus, the algorithm can effectively be implemented for the design of online complex PQ monitoring devices.

TABLE 8. Mathematical Modeling of Simulated Complex PQ Disturbances [29].

PQ Disturbance	Class symbol	Mathematical model	Parameters	
			Standard	Simulated
Sag + harmonics	C1	$V(t) = (1-\alpha(u(t-t_1)-u(t-t_2)))sin(\omega t)+\alpha_3 sin(\omega t)+\alpha_5 sin(\omega t)+\alpha_7 sin(\omega t)$	$\omega = 2\pi f; 0.1 \leq \alpha \leq 0.9, T \leq t_2-t_1 \leq 9T; 0.1 \leq \alpha_3, \alpha_5, \alpha_7 \leq 0.15$	$f = 50Hz; \alpha = 0.3, t_1 = 0.06, t_2 = 0.14; \alpha_3 = 0.05, \alpha_5 = 0.10, \alpha_7 = 0.15$
Swell + harmonics	C2	$V(t) = (1+\alpha(u(t-t_1)-u(t-t_2)))sin(\omega t)+\alpha_3 sin(\omega t)+\alpha_5 sin(\omega t)+\alpha_7 sin(\omega t)$	$\omega = 2\pi f; 0.1 \leq \alpha \leq 0.9, T \leq t_2-t_1 \leq 9T; 0.1 \leq \alpha_3, \alpha_5, \alpha_7 \leq 0.15$	$f = 50Hz; \alpha = 0.3, t_1 = 0.06, t_2 = 0.14; \alpha_3 = 0.05, \alpha_5 = 0.10, \alpha_7 = 0.15$
Interruption + harmonics	C3	$V(t) = (1-\alpha(u(t-t_1)-u(t-t_2)))sin(\omega t)+\alpha_3 sin(\omega t)+\alpha_5 sin(\omega t)+\alpha_7 sin(\omega t)$	$0.9 \leq \alpha \leq 1.0, T \leq t_2-t_1 \leq 9T; 0.1 \leq \alpha_3, \alpha_5, \alpha_7 \leq 0.15$	$\alpha = 0.95, t_1 = 0.06, t_2 = 0.14; \alpha_3 = 0.05, \alpha_5 = 0.10, \alpha_7 = 0.15$
Flicker + harmonics	C4	$V(t) = (1+\alpha_f sin(\beta\omega t))sin(\omega t)+\alpha_3 sin(\omega t)+\alpha_5 sin(\omega t)+\alpha_7 sin(\omega t)$	$0.1 \leq \alpha_f \leq 0.2,5 \leq \beta \leq 20Hz; 0.1 \leq \alpha_3, \alpha_5, \alpha_7 \leq 0.15$	$\alpha_f = 0.15, \beta = 15; \alpha_3 = 0.05, \alpha_5 = 0.10, \alpha_7 = 0.15$
Sag + OT	C5	$V(t) = (1-\alpha_1(u(t-t_1)-u(t-t_2)))sin(\omega t)+\alpha_2 e^{\frac{(t-t_3)}{\tau}} sin\omega_n(t-t_3)\{u(t_4-u(t_3))\}$	$0.1 \leq \alpha_1 \leq 0.9, T \leq t_2-t_1 \leq 9T; 0.1 \leq \alpha_2 \leq 0.8, 0.05T \leq t_4-t_3 \leq 3T, 8ms \leq \tau \leq 40ms, 300 \leq f_n \leq 900Hz$	$\alpha_1 = 0.3, t_1 = 0.06, t_2 = 0.14; \alpha_2 = 0.8, t_3 = 0.09, \tau = 0.02, t_4 = 0.11, f_n = 400Hz$
Swell + OT	C6	$V(t) = (1+\alpha_1(u(t-t_1)-u(t-t_2)))sin(\omega t)+\alpha_2 e^{\frac{(t-t_3)}{\tau}} sin\omega_n(t-t_3)\{u(t_4-u(t_3))\}$	$0.1 \leq \alpha_1 \leq 0.9, T \leq t_2-t_1 \leq 9T; 0.1 \leq \alpha_2 \leq 0.8, 0.05T \leq t_4-t_3 \leq 3T, 8ms \leq \tau \leq 40ms, 300 \leq f_n \leq 900Hz$	$\alpha_1 = 0.3, t_1 = 0.06, t_2 = 0.14; \alpha_2 = 0.8, t_3 = 0.09, \tau = 0.02, t_4 = 0.11, f_n = 400Hz$
Flicker + OT	C7	$V(t) = (1+\alpha_f sin(\beta\omega t))sin(\omega t)+\alpha e^{\frac{(t-t_1)}{\tau}} sin\omega_n(t-t_1)\{u(t_2-u(t_1))\}$	$0.1 \leq \alpha_f \leq 0.2,5 \leq \beta \leq 20Hz; 0.1 \leq \alpha \leq 0.8, 0.05T \leq t_2-t_1 \leq 3T, 8ms \leq \tau \leq 40ms, 300 \leq f_n \leq 900Hz$	$\alpha_f = 0.15, \beta = 15; \alpha = 0.8, t_1 = 0.08, \tau = 0.02, t_2 = 0.10, f_n = 400Hz$
Harmonics + OT	C8	$V(t) = sin(\omega t)+\alpha_3 sin(\omega t)+\alpha_5 sin(\omega t)+\alpha_7 sin(\omega t)+\alpha e^{\frac{(t-t_1)}{\tau}} sin\omega_n(t-t_1)\{u(t_2-u(t_1))\}$	$0.1 \leq \alpha_3, \alpha_5, \alpha_7 \leq 0.15; 0.1 \leq \alpha \leq 0.8, 0.05T \leq t_2-t_1 \leq 3T, 8ms \leq \tau \leq 40ms, 300 \leq f_n \leq 900Hz$	$\alpha_3 = 0.05, \alpha_5 = 0.10, \alpha_7 = 0.15; \alpha = 0.8, t_1 = 0.08, \tau = 0.02, t_2 = 0.10, f_n = 400Hz$
Sag + IT	C9	$V(t) = (1-\alpha_1(u(t-t_1)-u(t-t_2)))sin(\omega t)+\alpha_2 e^{\frac{(t-t_3)}{\tau}} - \alpha_2 e^{\frac{(t-t_3)}{\tau}}\{u(t_4-u(t_3))\}$	$0.1 \leq \alpha_1 \leq 0.9, T \leq t_2-t_1 \leq 9T; 1 \leq \alpha_2 \leq 10, 0.05T \leq t_4-t_3 \leq 3T, 8ms \leq \tau \leq 40ms$	$\alpha_1 = 0.3, t_1 = 0.06, t_2 = 0.14; \alpha_2 = 10, t_3 = 0.098, \tau = 0.02, t_4 = 0.101$
Swell + IT	C10	$V(t) = (1+\alpha_1(u(t-t_1)-u(t-t_2)))sin(\omega t)+\alpha_2 e^{\frac{(t-t_3)}{\tau}} - \alpha_2 e^{\frac{(t-t_3)}{\tau}}\{u(t_4-u(t_3))\}$	$0.1 \leq \alpha_1 \leq 0.9, T \leq t_2-t_1 \leq 9T; 1 \leq \alpha_2 \leq 10, 0.05T \leq t_4-t_3 \leq 3T, 8ms \leq \tau \leq 40ms$	$\alpha_1 = 0.3, t_1 = 0.06, t_2 = 0.14; \alpha_2 = 10, t_3 = 0.098, \tau = 0.02, t_4 = 0.101$
Flicker + IT	C11	$V(t) = (1+\alpha_f sin(\beta\omega t))sin(\omega t)+\alpha e^{\frac{(t-t_1)}{\tau}} - \alpha e^{\frac{(t-t_1)}{\tau}}\{u(t_2-u(t_1))\}$	$0.1 \leq \alpha_f \leq 0.2,5 \leq \beta \leq 20Hz; 1 \leq \alpha \leq 10, 0.05T \leq t_2-t_1 \leq 3T, 8ms \leq \tau \leq 40ms$	$\alpha_f = 0.15, \beta = 15; \alpha = 10, t_1 = 0.085, \tau = 0.02, t_2 = 0.088$
Harmonics + IT	C12	$V(t) = sin(\omega t)+\alpha_3 sin(\omega t)+\alpha_5 sin(\omega t)+\alpha_7 sin(\omega t)+\alpha e^{\frac{(t-t_1)}{\tau}} - \alpha e^{\frac{(t-t_1)}{\tau}}\{u(t_2-u(t_1))\}$	$0.1 \leq \alpha_3, \alpha_5, \alpha_7 \leq 0.15; 1 \leq \alpha \leq 10, 0.05T \leq t_2-t_1 \leq 3T, 8ms \leq \tau \leq 40ms$	$\alpha_3 = 0.05, \alpha_5 = 0.10, \alpha_7 = 0.15; \alpha = 10, t_1 = 0.085, \tau = 0.02, t_2 = 0.088$
Sag+spike	C13	$V(t) = (1-\alpha(u(t-t_1)-u(t-t_2)))sin(\omega t) + sign(sin(\omega t)) \times \left[\sum_{n=0}^{9} K \times \{u(t-(t_3+0.02n))-u(t-(t_4+0.02n))\}\right]$	$0.1 \leq \alpha \leq 0.9, T \leq t_2-t_1 \leq 9T; 0.1 \leq K \leq 0.4, 0 \leq t_3, t_4 \leq 0.5T, 0.01T \leq t_4-t_3 \leq 0.05T$	$\alpha = 0.3, t_1 = 0.06, t_2 = 0.14; K = 0.4, t_3 = 0.002, t_4 = 0.0023$
Sag + notch	C14	$V(t) = (1-\alpha(u(t-t_1)-u(t-t_2)))sin(\omega t) - sign(sin(\omega t)) \times \left[\sum_{n=0}^{9} K \times \{u(t-(t_3+0.02n))-u(t-(t_4+0.02n))\}\right]$	$0.1 \leq \alpha \leq 0.9, T \leq t_2-t_1 \leq 9T; 0.1 \leq K \leq 0.4, 0 \leq t_3, t_4 \leq 0.5T, 0.01T \leq t_4-t_3 \leq 0.05T$	$\alpha = 0.3, t_1 = 0.06, t_2 = 0.14; K = 0.4, t_3 = 0.006, t_4 = 0.0065$
Sag + OT + harmonics	C15	$V(t) = (1-\alpha_1(u(t-t_1)-u(t-t_2)))sin(\omega t)+\alpha_2 e^{\frac{(t-t_3)}{\tau}} sin\omega_n(t-t_3)\{u(t_4-u(t_3))\}+\alpha_3 sin(\omega t)+\alpha_5 sin(\omega t)+\alpha_7 sin(\omega t)$	$0.1 \leq \alpha_1 \leq 0.9, T \leq t_2-t_1 \leq 9T; 0.1 \leq \alpha_2 \leq 0.8, 0.05T \leq t_4-t_3 \leq 3T, 8ms \leq \tau \leq 40ms, 300 \leq f_n \leq 900Hz; 0.1 \leq \alpha_3, \alpha_5, \alpha_7 \leq 0.15$	$\alpha_1 = 0.3, t_1 = 0.04, t_2 = 0.14; \alpha_2 = 0.8, t_3 = 0.09, \tau = 0.02, t_4 = 0.11, f_n = 400Hz; \alpha_3 = 0.05, \alpha_5 = 0.10, \alpha_7 = 0.15$
Swell + OT + harmonics	C16	$V(t) = (1+\alpha_1(u(t-t_1)-u(t-t_2)))sin(\omega t)+\alpha_2 e^{\frac{(t-t_3)}{\tau}} sin\omega_n(t-t_3)\{u(t_4-u(t_3))\}+\alpha_3 sin(\omega t)+\alpha_5 sin(\omega t)+\alpha_7 sin(\omega t)$	$0.1 \leq \alpha_1 \leq 0.9, T \leq t_2-t_1 \leq 9T; 0.1 \leq \alpha_2 \leq 0.8, 0.05T \leq t_4-t_3 \leq 3T, 8ms \leq \tau \leq 40ms, 300 \leq f_n \leq 900Hz; 0.1 \leq \alpha_3, \alpha_5, \alpha_7 \leq 0.15$	$\alpha_1 = 0.3, t_1 = 0.04, t_2 = 0.14; \alpha_2 = 0.8, t_3 = 0.09, \tau = 0.02, t_4 = 0.11, f_n = 400Hz; \alpha_3 = 0.05, \alpha_5 = 0.10, \alpha_7 = 0.15$
Flicker + harmonics + IT	C17	$V(t) = (1+\alpha_f sin(\beta\omega t))sin(\omega t)+\alpha_3 sin(\omega t)+\alpha_5 sin(\omega t)+\alpha_7 sin(\omega t)+\alpha e^{\frac{(t-t_1)}{\tau}} - \alpha e^{\frac{(t-t_1)}{\tau}}\{u(t_2-u(t_1))\}$	$0.1 \leq \alpha_f \leq 0.2,5 \leq \beta \leq 20Hz; 0.1 \leq \alpha_3, \alpha_5, \alpha_7 \leq 0.15; 1 \leq \alpha \leq 10, 0.05T \leq t_2-t_1 \leq 3T, 8ms \leq \tau \leq 40ms$	$\alpha_f = 0.15, \beta = 15; \alpha_3 = 0.05, \alpha_5 = 0.10, \alpha_7 = 0.15; \alpha = 10, t_1 = 0.085, \tau = 0.02, t_2 = 0.088$
Sag + OT + harmonics + IT	C18	$V(t) = (1-\alpha_1(u(t-t_1)-u(t-t_2)))sin(\omega t)+\alpha_2 e^{\frac{(t-t_3)}{\tau_1}} sin\omega_n(t-t_3)\{u(t_4-u(t_3))\}+\alpha_3 sin(\omega t)+\alpha_5 sin(\omega t)+\alpha_7 sin(\omega t)+\beta e^{\frac{(t-t_5)}{\tau_2}} - \beta e^{\frac{(t-t_5)}{\tau_2}}\{u(t_6-u(t_5))\}$	$0.1 \leq \alpha_1 \leq 0.9, T \leq t_2-t_1 \leq 9T; 0.1 \leq \alpha_2 \leq 0.8, 0.05T \leq t_4-t_3 \leq 3T, 8ms \leq \tau_1 \leq 40ms, 300 \leq f_n \leq 900Hz; 0.1 \leq \alpha_3, \alpha_5, \alpha_7 \leq 0.15; 1 \leq \beta \leq 10, 0.05T \leq t_6-t_5 \leq 3T, 8ms \leq \tau_2 \leq 40ms$	$\alpha_1 = 0.3, t_1 = 0.06, t_2 = 0.14; \alpha_2 = 0.8, t_3 = 0.09, \tau_1 = 0.02, t_4 = 0.11, f_n = 400Hz; \alpha_3 = 0.05, \alpha_5 = 0.10, \alpha_7 = 0.15; \beta = 10, t_5 = 0.098, \tau_2 = 0.02, t_6 = 0.101$

APPENDIX

The mathematical modelling of the generated complex PQ disturbances, their standard and simulated parameters are provided in Table 8.

REFERENCES

[1] B. Biswal, P. K. Dash, and B. K. Panigrahi, "Power quality disturbance classification using fuzzy C-Means algorithm and adaptive particle swarm optimization," *IEEE Trans. Ind. Electron.*, vol. 56, no. 1, pp. 212–220, Jan. 2009.

[2] Q. Fu, L. F. Montoya, A. Solanki, A. Nasiri, V. Bhavaraju, T. Abdallah, and D. C. Yu, "Microgrid generation capacity design with renewables and energy storage addressing power quality and surety," *IEEE Trans. Smart Grid*, vol. 3, no. 4, pp. 2019–2027, Dec. 2012.

[3] M. Uyar, S. Yildirim, and M. T. Gencoglu, "An effective wavelet-based feature extraction method for classification of power quality disturbance signals," *Electr. Power Syst. Res.*, vol. 78, no. 10, pp. 1747–1755, Oct. 2008. [Online]. Available: http://www.sciencedirect.com/science/article/pii/S0378779608000953

[4] M. A. S. Masoum, S. Jamali, and N. Ghaffarzadeh, "Detection and classification of power quality disturbances using discrete wavelet transform and wavelet networks," *IET Sci., Meas. Technol.*, vol. 4, no. 4, pp. 193–205, Jul. 2010.

[5] P. K. Dash, B. K. Panigrahi, D. K. Sahoo, and G. Panda, "Power quality disturbance data compression, detection, and classification using integrated spline wavelet and S-transform," *IEEE Trans. Power Del.*, vol. 18, no. 2, pp. 595–600, Apr. 2003.

[6] O. P. Mahela, A. G. Shaik, and N. Gupta, "A critical review of detection and classification of power quality events," *Renew. Sustain. Energy Rev.*, vol. 41, pp. 495–505, Jan. 2015. [Online]. Available: http://www.sciencedirect.com/science/article/pii/S1364032114007564

[7] M. J. B. Reddy, R. K. Raghupathy, K. P. Venkatesh, and D. K. Mohanta, "Power quality analysis using discrete orthogonal S-transform (DOST)," *Digit. Signal Process.*, vol. 23, no. 2, pp. 616–626, Mar. 2013. [Online]. Available: http://www.sciencedirect.com/science/article/pii/S1051200412002321

[8] M. Valtierra-Rodriguez, R. de Jesus Romero-Troncoso, R. A. Osornio-Rios, and A. Garcia-Perez, "Detection and classification of single and combined power quality disturbances using neural networks," *IEEE Trans. Ind. Electron.*, vol. 61, no. 5, pp. 2473–2482, May 2014.

[9] R. Kumar, B. Singh, D. T. Shahani, A. Chandra, and K. Al-Haddad, "Recognition of power-quality disturbances using S-Transform-Based ANN classifier and rule-based decision tree," *IEEE Trans. Ind. Appl.*, vol. 51, no. 2, pp. 1249–1258, Mar. 2015.
[10] S. Mishra, C. N. Bhende, and B. K. Panigrahi, "Detection and classification of power quality disturbances using S-Transform and probabilistic neural network," *IEEE Trans. Power Del.*, vol. 23, no. 1, pp. 280–287, Jan. 2008.
[11] C. N. Bhende, S. Mishra, and B. K. Panigrahi, "Detection and classification of power quality disturbances using S-transform and modular neural network," *Electr. Power Syst. Res.*, vol. 78, no. 1, pp. 122–128, Jan. 2008. [Online]. Available: http://www.sciencedirect.com/science/article/pii/S0378779607000065
[12] T. Nguyen and Y. Liao, "Power quality disturbance classification utilizing S-transform and binary feature matrix method," *Electric Power Syst. Res.*, vol. 79, no. 4, pp. 569–575, Apr. 2009. [Online]. Available: http://www.sciencedirect.com/science/article/pii/S0378779608002320
[13] M. Uyar, S. Yildirim, and M. T. Gencoglu, "An expert system based on S-transform and neural network for automatic classification of power quality disturbances," *Expert Syst. Appl.*, vol. 36, no. 3, pp. 5962–5975, Apr. 2009. [Online]. Available: http://www.sciencedirect.com/science/article/pii/S0957417408004363
[14] H. S. Behera, P. K. Dash, and B. Biswal, "Power quality time series data mining using S-transform and fuzzy expert system," *Appl. Soft Comput.*, vol. 10, no. 3, pp. 945–955, Jun. 2010. [Online]. Available: http://www.sciencedirect.com/science/article/pii/S1568494609002038
[15] H. Shareef, A. Mohamed, and A. A. Ibrahim, "An image processing based method for power quality event identification," *Int. J. Electr. Power Energy Syst.*, vol. 46, pp. 184–197, Mar. 2013. [Online]. Available: http://www.sciencedirect.com/science/article/pii/S0142061512006126
[16] H. Erişti, Ö. Yıldırım, B. Erişti, and Y. Demir, "Automatic recognition system of underlying causes of power quality disturbances based on S-transform and extreme learning machine," *Int. J. Electr. Power Energy Syst.*, vol. 61, pp. 553–562, Oct. 2014. [Online]. Available: http://www.sciencedirect.com/science/article/pii/S0142061514001938
[17] Y.-L. Chen, H.-W. Hu, and K. Tang, "Constructing a decision tree from data with hierarchical class labels," *Expert Syst. Appl.*, vol. 36, no. 3, pp. 4838–4847, Apr. 2009. [Online]. Available: http://www.sciencedirect.com/science/article/pii/S095741740800273X
[18] O. P. Mahela and A. G. Shaik, "Recognition of power quality disturbances using S-transform and rule-based decision tree," in *Proc. IEEE 1st Int. Conf. Power Electron., Intell. Control Energy Syst. (ICPEICES)*, Jul. 2016, pp. 1–6.
[19] O. P. Mahela, B. Khan, H. H. Alhelou, and P. Siano, "Power quality assessment and event detection in distribution network with wind energy penetration using stockwell transform and fuzzy clustering," *IEEE Trans. Ind. Informat.*, vol. 16, no. 11, pp. 6922–6932, Nov. 2020.
[20] O. P. Mahela and A. G. Shaik, "Recognition of power quality disturbances using S-transform and fuzzy C-means clustering," in *Proc. Int. Conf. Cogeneration, Small Power Plants District Energy (ICUE)*, Sep. 2016, pp. 1–6.
[21] T. Zhong, S. Zhang, G. Cai, Y. Li, B. Yang, and Y. Chen, "Power quality disturbance recognition based on multiresolution S-transform and decision tree," *IEEE Access*, vol. 7, pp. 88380–88392, 2019.
[22] O. P. Mahela, B. Khan, H. Haes Alhelou, and S. Tanwar, "Assessment of power quality in the utility grid integrated with wind energy generation," *IET Power Electron.*, to be published. [Online]. Available: https://digital-library.theiet.org/content/journals/10.1049/iet-pel.2019.1351, doi: 10.1049/iet-pel.2019.1351.
[23] L. Lin, D. Wang, S. Zhao, L. Chen, and N. Huang, "Power quality disturbance feature selection and pattern recognition based on image enhancement techniques," *IEEE Access*, vol. 7, pp. 67889–67904, 2019.
[24] O. P. Mahela and A. G. Shaik, "Recognition of power quality disturbances using S-transform based ruled decision tree and fuzzy C-means clustering classifiers," *Appl. Soft Comput.*, vol. 59, pp. 243–257, Oct. 2017. [Online]. Available: http://www.sciencedirect.com/science/article/pii/S1568494617303393
[25] W.-M. Lin, C.-H. Wu, C.-H. Lin, and F.-S. Cheng, "Detection and classification of multiple power-quality disturbances with wavelet multiclass SVM," *IEEE Trans. Power Del.*, vol. 23, no. 4, pp. 2575–2582, Oct. 2008.
[26] M. A. A. Lima, A. S. Cerqueira, D. V. Coury, and C. A. Duque, "A novel method for power quality multiple disturbance decomposition based on independent component analysis," *Int. J. Electr. Power Energy Syst.*, vol. 42, no. 1, pp. 593–604, Nov. 2012. [Online]. Available: http://www.sciencedirect.com/science/article/pii/S0142061512001949
[27] S. Dalai, D. Dey, B. Chatterjee, S. Chakravorti, and K. Bhattacharya, "Cross-spectrum analysis-based scheme for multiple power quality disturbance sensing device," *IEEE Sensors J.*, vol. 15, no. 7, pp. 3989–3997, Jul. 2015.
[28] *Recommended Practice for Monitoring Electric Power Quality*, Standard IEEE 1159:1995, 2019.
[29] R. H. G. Tan and V. K. Ramachandaramurthy, "Numerical model framework of power quality events," *Eur. J. Sci. Res.*, vol. 43, no. 1, pp. 30–47, Jun. 2010.
[30] B. K. Panigrahi, P. K. Dash, and J. B. V. Reddy, "Hybrid signal processing and machine intelligence techniques for detection, quantification and classification of power quality disturbances," *Eng. Appl. Artif. Intell.*, vol. 22, no. 3, pp. 442–454, Apr. 2009. [Online]. Available: http://www.sciencedirect.com/science/article/pii/S0952197608001486
[31] P. K. Ray, N. Kishor, and S. R. Mohanty, "Islanding and power quality disturbance detection in grid-connected hybrid power system using wavelet and *S*-transform," *IEEE Trans. Smart Grid*, vol. 3, no. 3, pp. 1082–1094, Sep. 2012.
[32] N. Huang, L. Lin, W. Huang, and J. Qi, "Review of power-quality disturbance recognition using S-transform," in *Proc. IITA Int. Conf. Control, Autom. Syst. Eng. (CASE)*, Jul. 2009, pp. 438–441.
[33] R. G. Stockwell, L. Mansinha, and R. P. Lowe, "Localization of the complex spectrum: The s transform," *IEEE Trans. Signal Process.*, vol. 44, no. 4, pp. 998–1001, Apr. 1996.
[34] H. Kerdegari, K. Samsudin, A. R. Ramli, and S. Mokaram, "Evaluation of fall detection classification approaches," in *Proc. 4th Int. Conf. Intell. Adv. Syst. (ICIAS)*, Jun. 2012, pp. 131–136.
[35] H. B. Mirza and V. R. Ratnaparkhe, "Classifier tools: A comparative study," in *Proc. 2nd Int. Conf. Intell. Comput. Control Syst. (ICICCS)*, Jun. 2018, pp. 1543–1547.
[36] O. P. Mahela and A. G. Shaik, "Power quality improvement in distribution network using DSTATCOM with battery energy storage system," *Int. J. Electr. Power Energy Syst.*, vol. 83, pp. 229–240, Dec. 2016. [Online]. Available: http://www.sciencedirect.com/science/article/pii/S0142061516306433
[37] Q. Xu, F. Ma, A. Luo, Z. He, and H. Xiao, "Analysis and control of M3C-based UPQC for power quality improvement in medium/high-voltage power grid," *IEEE Trans. Power Electron.*, vol. 31, no. 12, pp. 8182–8194, Dec. 2016.
[38] A. Javadi and K. Al-Haddad, "A single-phase active device for power quality improvement of electrified transportation," *IEEE Trans. Ind. Electron.*, vol. 62, no. 5, pp. 3033–3041, May 2015.

OM PRAKASH MAHELA (Senior Member, IEEE) was born in Sabalpura, Kuchaman, Rajasthan, India, in 1977. He received the B.E. degree from the College of Technology and Engineering, Udaipur, India, in 2002, the M.Tech. degree from Jagannath University, Jaipur, India, in 2013, and the Ph.D. degree from IIT Jodhpur, India, in 2018, all in electrical engineering. From 2002 to 2004, he was an Assistant Professor with the Rajasthan Institute of Engineering and Technology, Jaipur. From 2004 to 2014, he was a Junior Engineer with the Rajasthan Rajya Vidyut Prasaran Nigam Ltd., India, where he has been an Assistant Engineer, since July 2014. He has authored more than 140 research articles and book chapters. He performed more than 100 reviews for the prestigious journals of IEEE, Elsevier, Springer, Willey, and Taylor & Francis. His research interests include power quality, power system planning, grid integration of renewable energy sources, FACTS devices, transmission line protection, and condition monitoring. He was a recipient of the University Rank Certificate in 2002, the Gold Medal in 2013, the Best Research Paper Award in 2018, and the C. V. Raman Gold Medal in 2019. He also received the certificates of outstanding contribution in the reviewing from *Computers and Electrical Engineering*, the *International Journal of Electrical Power and Energy Systems*, *Measurement*, and *Renewable and Sustainable Energy Reviews*.

ABDUL GAFOOR SHAIK (Member, IEEE) received the Ph.D. degree in power systems. He is currently an Associate Professor with the Department of Electrical Engineering, IIT Jodhpur. He has an industrial and academic research experience of more than 20 years. He has published over 50 research articles in reputed journals, international conferences, and book chapters. He has wide research experience in the area of power system protection and power quality. His research interests include the development of power system protection algorithms using multi-resolution analysis, such as wavelet transform and S-transform and power quality mitigation in distribution networks with RE sources using adaptive control algorithms. The courses taught by him include power system protection, electrical machines, power systems, power electronics, smart grid, and basic electrical engineering. He always excelled in academics and awarded the Gold Medal at Graduate and Post Graduate level. He was a recipient of the Best Paper Award from the Institution of Engineers, India, in 2015. His core team comprises of highly skilled students pursuing master's and Ph.D. degrees in the area of power quality, induction motor protection, power system protection, and smart grid.

BASEEM KHAN (Member, IEEE) received the Bachelor of Engineering degree in electrical engineering from Rajiv Gandhi Technological University, Bhopal, India, in 2008, and the Master of Technology and Doctor of Philosophy degrees in electrical engineering from the Maulana Azad National Institute of Technology, Bhopal, India, in 2010 and 2014, respectively. He is currently working as a Faculty Member with Hawassa University, Ethiopia. His research interests include power system restructuring, power system planning, smart grid technologies, meta-heuristic optimization techniques, reliability analysis of renewable energy systems, power quality analysis, and renewable energy integration.

RAJENDRA MAHLA (Student Member, IEEE) was born in Sabalpura, Kuchaman, Rajasthan, India, in 2000. He is currently pursuing the Bachelor of Technology degree with the National Institute of Technology at Kurukshetra, Kurukshetra, India. He has authored one research article in International Journal. His research interests include power quality, grid integration of renewable energy, and transmission line protection. He qualified the Joint Entrance Examination (Mains and Advanced), in 2018.

HASSAN HAES ALHELOU (Member, IEEE) is currently a Faculty Member with Tisheen University, Lattakia, Syria. He has published more than 30 research articles in the high quality peer-reviewed journals and international conferences. He has also performed more than 160 reviews for high-prestigious journals, including the IEEE TRANSACTIONS ON INDUSTRIAL INFORMATICS, the IEEE TRANSACTIONS ON INDUSTRIAL ELECTRONICS, *Energy Conversion and Management*, *Applied Energy*, and the *International Journal of Electrical Power and Energy Systems*. He has participated in more than 15 industrial projects. His major research interests include power systems, power system dynamics, power system operation and control, dynamic state estimation, frequency control, smart grids, micro-grids, demand response, load shedding, and power system protection. He is included in the 2018 and 2019 Publons list of the top 1% Best Reviewer and researchers in the field of engineering. He was a recipient of the Outstanding Reviewer Award of *Energy Conversion and Management* journal in 2016, the *ISA Transactions* journal in 2018, and *Applied Energy* journal in 2019, and many other Awards. He was a recipient of the Best Young Researcher in the Arab Student Forum Creative among 61 researchers from 16 countries at Alexandria University, Egypt, in 2011.